# Evaluation of wild type and mutants of β-Glucuronidase (GUS) against natural and synthetic substrates

A Thesis Submitted to the College of Graduate Studies and Research
In Partial Fulfillment of the Requirements
For the degree of Master of Science
In the Department of Chemistry
University of Saskatchewan
Saskatoon, SK

By Siddharth Tiwari

## PERMISSION TO USE

In presenting this thesis in partial fulfillment of the requirements for a postgraduate degree from the University of Saskatchewan, I agree that the libraries of this University may make it freely available for inspection. I further agree that permission for copying of this thesis in any manner, in whole or in part, for scholarly purposes may be granted by the professor or professors who supervised my thesis work or, in their absence, by the department Head of the Department or the Dean of the College in which my thesis work was done. It is understood that any copy or publication or use of this thesis or parts thereof for financial gain shall not be allowed without my written permission. It is also understood that due recognition shall be given to me and to the University of Saskatchewan in any use which may be made of any material in my thesis.

Requests for permission to reproduce or to make use of materials in the thesis in whole or in part should be directed to:

Head of the Department of Chemistry

University of Saskatchewan

110 Science Place

Saskatoon, Saskatchewan

S7N 5C9 CANADA

## ABSTRACT

Modifying substrate specificity of β-glucuronidase (GUS) would be helpful in various enzyme prodrug systems in delivering drug dose to the site of action in the cancer treatment. Due to the presence of endogenous enzyme in human tissues, GUS-based Antibody-directed Enzyme Prodrug Therapy (ADEPT) requires a novel substrate to avoid undesirable systemic activation. GUS is a glycosyl hydrolase, highly specific towards the glucuronide derivatives. It catalyzes the glycosidic cleavage of β-D-glucuronides to β-D-glucuronic acid and aglycone moiety. In order to gain insight on the substrate specificity of GUS, C6 carboxyl group of glucuronic acid was modified to C6 carboxamide (amide derivative). We have examined amide derivatized substrates with a variety of different aglycone groups including *p*-nitrophenyl, phenyl and 4-methylumbelliferone to further probe the activity profile of GUS. In an effort to optimize GUS activity, docking studies have been performed which indicated that amino acid point mutations near C6 carboxyl group of glucuronic acid could improve binding of the derivatized substrates. As a result point mutations to Arg-562 and Lys-568 which make the active site less positively charged either by glutamine or glutamate lead to an enzyme with much lower native substrate activity but abolished activity for the amide-derivatized substrate. This research study showed that there is still a further need of finding appropriate mutations required to make glucuronamide a better substrate for the mutated version of GUS.

## ACKNOWLEDGEMENTS

First and foremost, I would like to express my sincere thanks to my supervisor Dr. David A. R. Sanders for his support, guidance, and patience throughout my time during this research. I would also like to acknowledge Sean Dalrymple for his helpful suggestions, discussions and encouragement during the course of this project. I think without you Sean this project would not have been possible. I would also like to thank Dr. David R.J. Palmer for his valuable suggestions and guidance. I am thankful to the members of the Sanders & Palmer research groups for their technical assistance. I acknowledge and thank the Department of Biochemistry and Saskatchewan Structural Sciences Center (SSSC) for their instrumentation and, more specifically Jason Maley and Michal Boniecki for their assistance. Thank you to the members of my advisory committee, Dr. Stephen Urquhart and Dr. Jens Mueller for their constructive criticism and helpful suggestions for this research.

I acknowledge and I am thankful for the financial contributions from the Canadian Breast Cancer Foundation and NSERC. I would also like to thank the College of Graduate Studies and Research, Department of Chemistry and University of Saskatchewan.

# TABLE OF CONTENTS

## LIST OF FIGURES

## LIST OF TABLES

## LIST OF SCHEMES

## LIST OF ABBREVIATIONS

| | |
|---|---|
| ADEPT | Antibody Directed Prodrug Therapy |
| BME | β-mercaptoethanol |
| CD | Circular dichroism |
| DNA | Deoxyribonucleic acid |
| *E. coli* | *Escherichia coli* |
| FDA | Food and drug administration |
| GA | Glucuronic acid |
| GDL | Glucaro-δ-lactam |
| GDEPT | Gene Directed Prodrug Therapy |
| GUS | β-Glucuronidase |
| HEPES | 2-[4-(2-hydroxyethyl)piperazin-1-yl]ethanesulfonic acid |
| IPTG | Isopropyl β-D-1-thiogalactopyranoside |
| ITC | Isothermal titration calorimetry |
| LB | Luria-Bertani |
| MU | 4-methylumbelliferone |
| OD | optical density |
| PCR | Polymerase chain reaction |
| PG | Phenyl-β-D-Glucuronide |
| PGun | Phenyl-β-D-Glucuronamide |
| PNPG | *p*-nitrophenyl-β-D-Glucuronide |
| PNPGun | *p*-nitrophenyl-β-D-Glucuronamide |
| SDS-PAGE | Sodium dodecyl sulfate polyacrylamide gel electrophoresis |
| VDEPT | Virus Directed Prodrug Therapy |
| Wt | Wild type |

# 1 INTRODUCTION

## 1.1 Targeted Cancer Therapy

Chemotherapy is often associated with cytotoxic side effects due to the nature of medicinal agents. Premature termination of chemotherapy often results due to the intolerable side effects. The majority of these medicinal agents lack the ability to discriminate between normal and cancerous cells. As a result, drug-induced toxicity prevents achieving effective therapeutic drug concentration at cancer tissues. Due to physiological similarities between normal and tumor cells, the clinical efficacy of most anti-tumor drugs is limited by concentration-dependent systemic toxicity[1]. The development of improved methods for selective delivery of medicinal agents for cancer treatment is an active area of research[1]. Selective targeting of cancer cells with potent drug molecules enables better efficacy of the treatment and reduces side effects due to less exposure of drug dose to the patient. There are a variety of cancer treatments involving targeted drug delivery systems such as liposomes, nanoparticles, dendrimers, polymersomes and carbon nanotubes utilizing cell surface receptors like transferrin, lactoferrin, folate, and human epidermal growth receptors (EGFR) to the tumor cells[2]. One way is to administer an inactive form of the drug which is referred to as prodrug (less toxic). This prodrug is only converted in to a potent active drug form through enzymatic reaction when it is near the tumor site with the aid of enzyme conjugated delivery system[3].

## 1.2 Enzyme Prodrug Delivery Systems

Enzyme prodrug delivery systems selectively activate prodrugs through enzymes which include systems like Antibody Directed Prodrug Therapy (ADEPT), Virus Directed Prodrug Therapy (VDEPT), and Gene Directed Prodrug Therapy (GDEPT)[4]. These delivery systems either involve selected enzyme accumulation in the tumor by directing the enzyme or enzyme expression in the tumor cells through targeted gene therapy.

### 1.2.1 Gene Directed Enzyme Prodrug Therapy (GDEPT)

GDEPT is a gene therapy based on introduction of DNA into the cells. Gene therapy involves viral and non-viral insertion of DNA into cells. It mainly aims on enzyme gene sequence. The

gene sequence is first introduced in the cancer cells via gene therapy[5]. Once the gene is introduced into the tumor cells, it results in subsequent enzyme expression. Successful enzyme expression is followed by prodrug administration to the patient. The enzyme specific to prodrug, activates the prodrug at the site of action. There are a variety of enzymes that have been used in GDEPT like cytosine deaminase[6], carboxypeptidase G2[7], and CYP450[8]. The major challenge in GDEPT is low gene transfer rate specifically to tumor cells *in vivo*, poor enzyme expression and low efficiency in terms of gene expression, and other problems like local infection and tumor nodule ulceration[4, 9].

### 1.2.2 Virus Directed Prodrug Therapy (VDEPT)

VDEPT involves viral vectors for introducing enzyme gene sequence into the tumor cells[4]. In other words, it is also known as Virus Based Gene Therapy[10]. Various adenoviral and retroviral vectors have been studied to optimize conditions for VDEPT[11]. One of the trials showed reduced tumor growth *in vitro* and *in vivo* using human type-5 adenovirus vector for expressing purine nucleoside phosphorylase, along with hormonal therapy[12]. The limitations of using adenovirus vectors is, they transduce both dividing and non-dividing cells, while retroviral vectors targets specifically to dividing cells[4]. Considering slowly dividing human tumor cells, retroviral vectors showed poor transduction rate for tumor targeting[13]. The main limitations of these vectors include immunogenicity, insertional mutagenesis to host cell DNA, and low transduction rate. As a result, these methods are still struggling to meet their objectives due to low transduction rate, results in poor enzyme expression in tumor cells[4, 9].

### 1.2.3 Antibody Directed Enzyme Prodrug Therapy (ADEPT)

The tumor antigen-specific delivery system involves an antibody–enzyme (Ab-Enz) conjugate, where the antibody is specific to an antigen expressed by tumor cells[14]. The enzyme specific to the prodrug, catalyzes the reaction. This results in the release of active drug near tumor cells. ADEPT involves a four step process (**Fig 1.1**) for which the first step is administration of an Ab-Enz conjugate to the patient. After binding of the conjugate to the tumor expressing the antigen, in step 2 excess Ab-Enz must be excreted prior to the next step *in vivo*. Prodrug is then administered in step 3 and become selectively activated (active form) at the site of the tumor by the enzymatic catalysis in step 4[3, 15] (**Fig 1.1**). The important feature of ADEPT is that it increases the active drug concentration near tumor vicinity which kills the tumor cells.

Major limitations that ADEPT is facing are immunogenicity issues of Ab-Enz conjugates, preactivation of prodrug and poor efficacy, which will be briefly discussed in later part of this thesis. Like other enzyme prodrug systems, ADEPT also struggling to fulfill its objectives so far. In order to optimize ADEPT and improve its efficacy, each component of it needs to be optimized. In this research a long term goal is to apply our basic research to an ADEPT system.

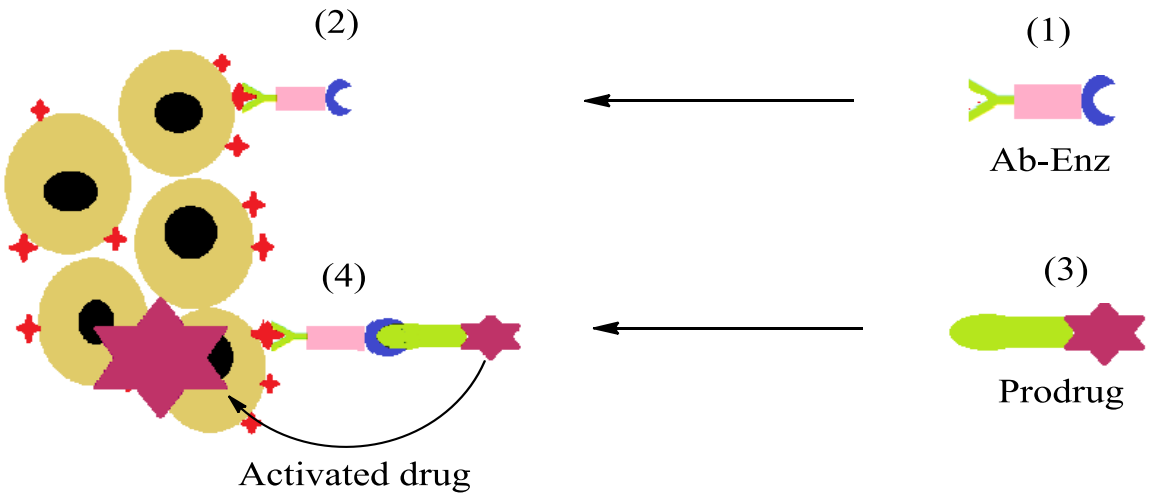


**Figure 1.1 Overview of steps involved in ADEPT:** (1) Ab-Enz conjugate is administered initially, (2) Ab-Enz binds to the specific to tumor antigen, (3) Prodrug is administered to the patient, (4) Prodrug is activated at the site of action

## 1.3 ADEPT Antibodies

Fundamental to the ADEPT approach is the specificity which exists between an antibody and its antigen. This is an important tool in cancer treatment[16, 17]. Monoclonal antibodies (mAbs) have been used for selective delivery of therapeutics against a particular tumor antigen and play a potential role for their use as delivery vehicles in bioactive or diagnostic agents. There are a number of different antibodies that are approved by FDA for various cancer types including Trastuzumab for breast cancer, Cetuximab and Bevacizumab for colorectal cancer, Ibritumomab tiuxetan and Rituximab for non-Hodgkin's lymphoma, Gemtuzumab ozogamicin for acute myelogenous leukemia, and Alemtuzumab for chronic lymphocytic leukemia[1, 16, 18]. Promising good results have been achieved by using mAbs in case of haematopoietic melignancies like non-Hodgkin's lymphoma[1]. The human epidermal growth receptors (EGFR/ HER) are expressed in various types of cancers, including breast cancer[18]. As overexpression of HER-2 in breast cancer is prominent, Trastuzumab (first anti HER2 mAb) showed promising results for

ADEPT[19, 20]. Some of limitations that do come across optimizing ADEPT system are, large size of antibodies, which leads to poor penetration of the conjugate in the tumor, and high intratumoural pressure which also acts as barrier for the conjugate to attach to the tumor[1, 19]. A recent study suggests that patients develop resistance against Trastuzumab for anti-HER2 treatment and there are several factors like angiogenesis, endocrine resistance, cell cycle regulators and other HER2 inhibitors that needs to be considered for optimizing anti-HER2 treatment[19, 20].

## 1.4 ADEPT Enzymes

The enzymes employed for prodrug activation conversion are fundamental to the ADEPT approach. In the literature to date, various enzymes have been examined including both mammalian and non-mammalian sources such as nitroreductase[21], carboxypeptidase A[22], β-lactamase[23], cytosine deaminase[13], carboxypeptidase G2[24], β-glucuronidase[25], alkaline phosphatase[26], α-galactosidase[27] and penicillin G amidase[28]. Enzymes from non-mammalian origin, prevent the unwanted activation of the prodrug by endogenous enzymes and catalyze the reaction more specifically to the tumor site. There are no post translational modification issues such as glycosylation and high scale production makes it easy to use[29]. A major disadvantage of using non-mammalian enzymes is elicitation of an immune response[30, 31]. In the case of mammalian enzymes, the potential chance for immune response is reduced but endogenously expressed enzyme can reduce specificity through systemic activation as a result preactivation of prodrug occurs resulting in failure of targeted drug delivery, loss of effective drug therpeutic index and side effects due to toxicity of drug to normal cells. Enzymes from non-mammalian sources which have mammalian homologues have been used such as β-glucuronidase, carboxypeptidase A and nitroreductase. Due to their non-mammalian origin, there will always be chances of an immune response. In case of Human β-glucuronidase (GUS), it is expressed endogenously and so is present in low levels in blood. Human GUS is less catalytic efficient compared to its bacterial form[29]. The optimum pH of Human GUS (pH range 4-5)[32] and bacterial GUS (pH range 5-7)[33] differ greatly. Human GUS (lysosomal acid hydrolase) exhibited only 10% activity at physiological pH[34]. Considering nitroreductase (NR), Human NR uses a different substrate compared to bacterial NR[29].

One of the clinical trials of ADEPT for colorectal cancer used caboxypeptidase G2 to activate a prodrug (bis-iodo phenol mustard, ZD2767P) and showed remarkable site specificity, giving tumor to blood ratios of antibody-enzyme conjugate (>10000 : 1), with few side effects [24]. Use of Ab-Enz conjugates with prodrugs showed promising results such as using glucuronylated Doxorubicin (DOX-GA3) as prodrug and Ab-Enz conjugate as 323/A3-mGUS using β-glucuronidase, demonstrated strong antitumor effect resulting growth inhibition of 93%[25].

GUS has been tested with glucuronide derivatives of a variety of drugs like doxorubicin[25], 9-amino-camptothecin[35], Epirubicine[36] and Aniline-mustard[37] as prodrugs and showed promising results and reduced systemic toxicity[38]. As GUS is present in human blood and tissues, there is potential for systemic activation of the prodrug [39]. There are a limited number of attempts carried out in the case of breast cancer[40] and various other studies done on cancer are still struggling to meet their objectives[41].

In most of the trials and studies for ADEPT, there were problems related to the side effects due to non-specificity of human enzyme analogues or immunogenicity issues associated with the use of enzyme of non-mammalian origin[42]. Bacterial enzymes that have no human analogue could provide high specificity and provide the advantage of higher turnover rates.

### 1.4.1 β-Glucuronidase

β-Glucuronidase (GUS, EC 3.2.1.31) is a type 2 glycoside hydrolase that catalyzes the cleavage of β-glucuronides[43]. The enzyme is highly specific for the carbohydrate moiety of the glucuronide substrate, while almost any aglycone moiety (or drug) can be conjugated to β-D-glucuronide moiety at C-1 hydroxyl (**Scheme 1**).

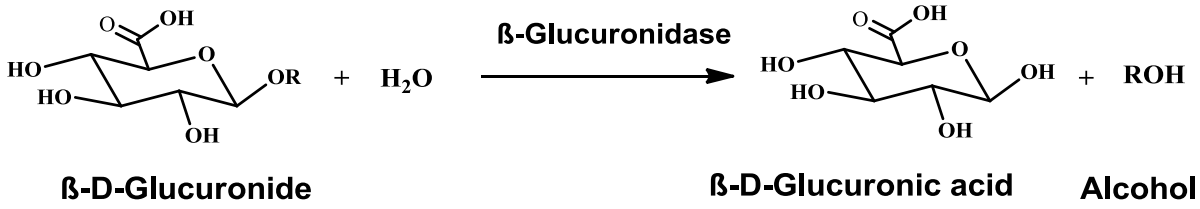


**Scheme 1 Hydrolysis of β-D-glucuronide derivative**

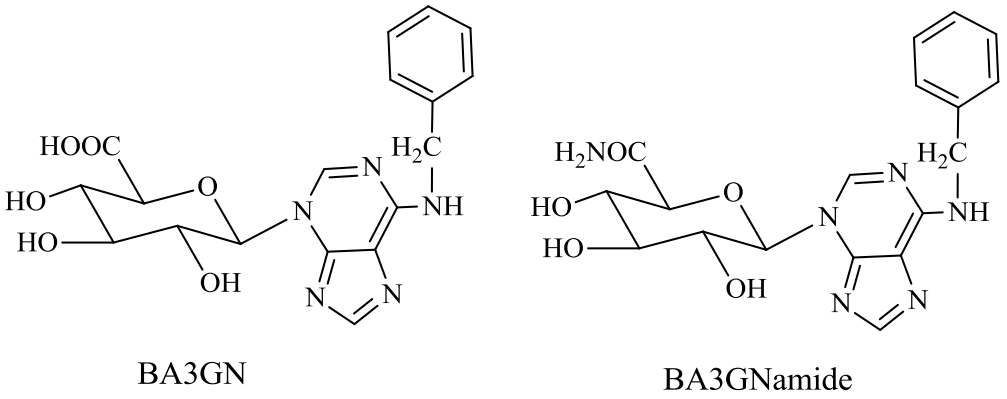


**Figure 1.2 Structure of substrate and non-substrate of GUS**. The compound on the left is BA3GN is a substrate for GUS while the compound on right is BA3GNamide is not a substrate.

GUS is highly active towards the C6 carboxylic acid of glucuronide moiety substrates, although it showed very reduced activity with galacturonide (C4 hydroxyl in opposite orientation), glucoside (C6 hydroxymethyl), galactoside (C4 hydroxyl in opposite orientation with C6 hydroxymethyl) and mannoside (C2 hydroxyl in opposite orientation)[44]. The reason behind high activity of GUS towards glucuronide moeities could be the putative negative charge of the C6 carboxyl group ionic interaction by positively charged residues[45]. The specificity of GUS towards the C6 carboxyl group makes it more specific for glucuronide derivatives. The glucuronamide that is not a substrate for GUS is Benzyladenine N3-glucuronamide (BA3GNamide). BA3GNamide was made from Benzyladenine N3-glucuronide (BA3GN) compound where the carboxylic acid was replaced by an amide group (**Fig 1.2**)[46].

### 1.4.2 Mechanism

The catalytic mechanism for GUS is a two-step process involving the formation and hydrolysis of a covalent glucuronyl-enzyme intermediate via oxacarbenium ion-like transition states[47]. In case of *Escherichia coli* (*E. coli*) GUS, the two catalytically important residues are E413 and E504, of which E504 acts as the catalytic nucleophile, while E413 act as a general acid/base (**Scheme 2**). In the first step of glucuronylation, E504 attacks at the C1 anomeric carbon, this leads to the release of the aglycone moiety with protonic assistance of E413, forming a glucuronyl-enzyme intermediate. In the second step, deglucuronylation proceeds via hydrolysis, where a water molecule acts as a nucleophile with base assistance of E413. This leads to the release of the glucuronic acid and returns the enzyme to its original state.

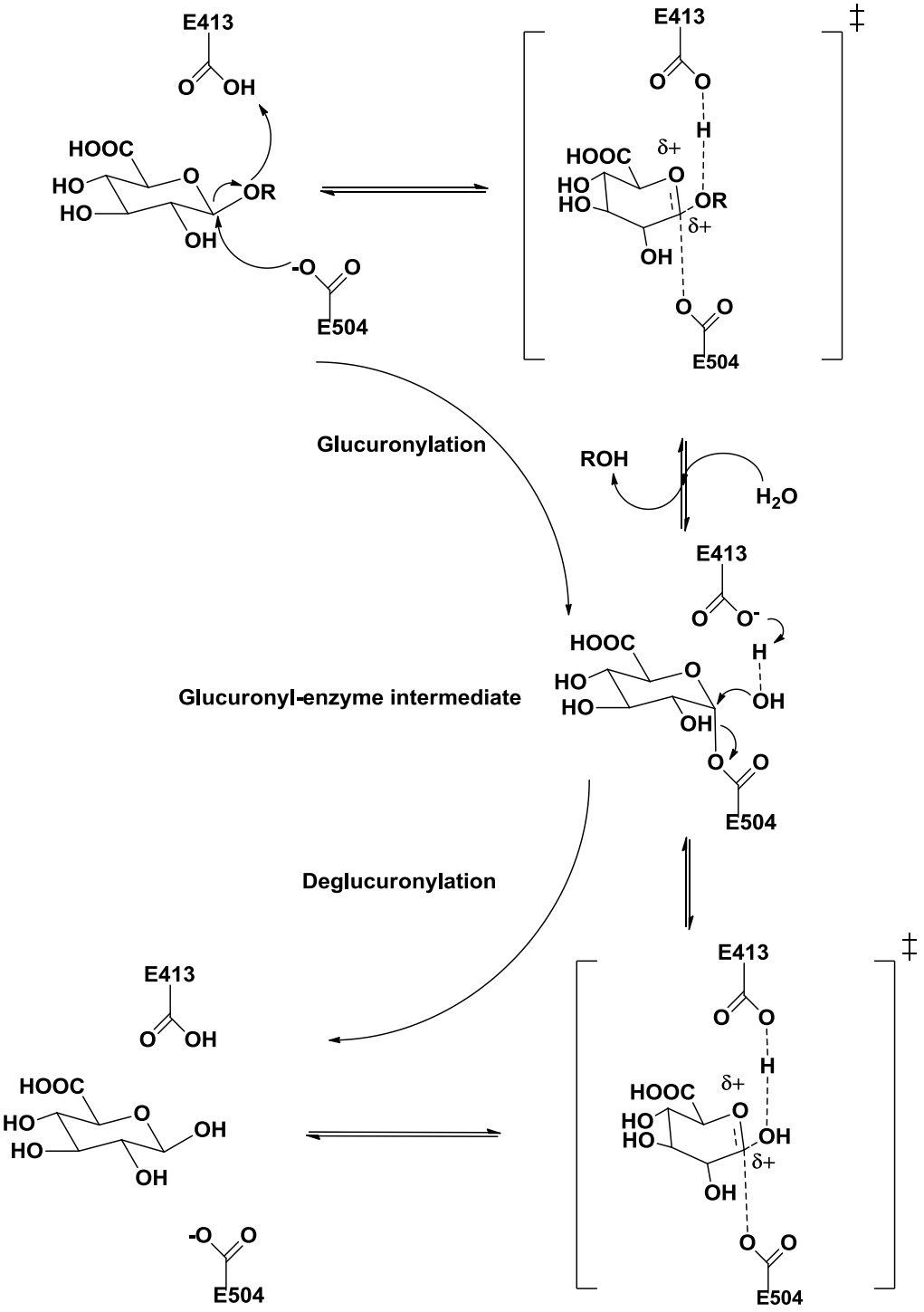


**Scheme 2 Mechanism of β-glucuronidase** [48].

### 1.4.3 GUS from Plants, animals and microorganisms

GUS catalyzes the reaction to give glucuronic acid, which is the fundamental component of proteoglycans like heparan sulphate, chondroitin sulphate, dermatan sulphate and hyluronan in animals while arabinogalactan in higher plants[49].

GUS is classified into three glycoside hydrolase (GH) families, GH1, GH2 and GH79, based on the amino acid sequence in the Carbohydrate-Active-Enzymes (CAZy) database (http://www.cazy.org/Glycoside-Hydrolases.html). No GUS from GH2 family or similar sequence have been found in plants[49]. The first ever GUS structure that was crystallized and solved was human GUS[50] followed by *E. coli* GUS[51]. *E. coli* and Human GUS structures belong to the GH2 family which reveals high sequence similarity.

*E. coli* GUS is a cytoplasmic enzyme with a broad pH range (pH 5.0 - 7.5)[33]. It exists as a homotetramer containing active site residues at the tetramer interface in a large cleft at the interface of two monomers with a monomer weight of 68 kDa [51, 52]. One of the attractive features for using *E. coli* GUS in ADEPT is its ability to tolerate large amino terminal fusions without loss of enzyme function and stability[33, 53]. *E. coli* GUS is also thermotolerant and resistant to many proteases[33, 53], which would be helpful in utilizing GUS in ADEPT.

Human GUS catalyzes degradation of glucuronic acid containing glucosaminoglycans like heparan sulphate, chondroitin sulphate, dermatan sulphate[54] and in proteoglycan degradation of lysosomes[55]. Lysosomes are membrane bound vacuoles responsible for digesting biomolecules such as sugars and proteins. As with *E. coli* GUS, its active form is a homotetramer where each monomer is 75-83 kDa[32, 56]. Deficiency of Human GUS leads to mucopolysaccharidosis Type VII which results in accumulation of mucopolysaccharides in body tissues[57]. After the glycosylation at *N*-glycosylation sites in the endoplasmic reticulum and Golgi complex, it is directed to lysosomes via mannose-6-phosphate receptor[58, 59]. The pH optimum for Human GUS is in the range of 4-5[32, 60], which is low compared to pH range of *E. coli* GUS, which suggests low turnover rate of Human GUS at physiological pH. It also possess thermotolerance and stability[32]. No cooperative binding in both *E. coli* and Human GUS has been reported yet.

### 1.4.4 Structural Features

The structure of Human and *E. coli* GUS both have been solved through X ray crystallography[50, 51, 61]. Human GUS was crystallized a decade ago, while *E. coli* GUS was crystallized recently and showed an overall 50% sequence similarity[50] (**Fig 1.3**) and were structurally very similar (**Fig 1.4**).

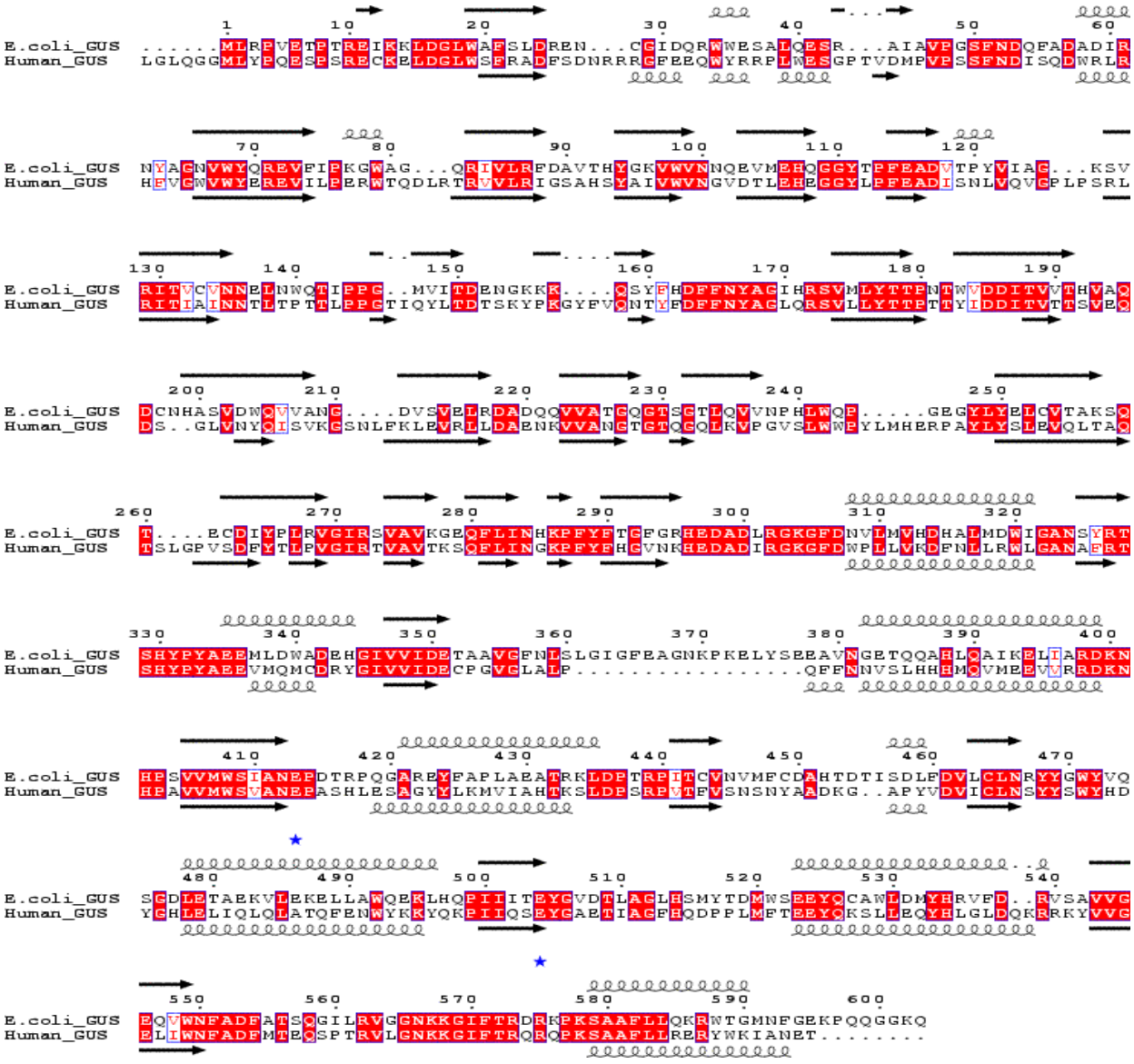


**Figure 1.3 Sequence alignment of *E. coli* GUS and human GUS**

Sequence alignment was performed by using *ClustalW* [62],Blosum scoring matrix[63, 64] and *ESPript* V2.2[65] Amino acids represented with white letters in red background are identical residues, while red letters represents similar residues. Secondary structures of *E. coli* GUS and Human GUS crystal structure are displayed above and below the sequence alignment respectively. Blue starred residues represent the conserved catalytic residues.

The overall structure contains two domains where the C-terminal domain forms the α/β- or TIM barrel motif containing the active site residues, and the N-terminal domain resembling the sugar binding motif of family 2 glycosyl hydrolases[51]. The active site residues in *E. coli* GUS are E504 and E413, respectively which corresponds to E540 and E451 in Human GUS. Additionally the region between the N- and C-terminal domains exhibit an immunoglobulin like β-sandwich domain consistent with other family 2 glycosyl hydrolases [66].

Superimposing Human and *E. coli* GUS structure reveals a 1.4 Å root mean square deviation (rmsd) over 565 equivalent Cα positions[51]. Interestingly the *E. coli* GUS structure contains a 17-residue "bacterial loop", not found in the human GUS. A recent study showed that, the bacterial loop is highly important for higher activity of GUS as well as for selective inhibition[61].

So far, there have been crystal structures of GUS with inhibitors, but no GUS structure with substrate or product has been crystallized yet. In an *E. coli* GUS, each active site contains two bacterial loops, one from the same monomer while other from the neighboring monomer (**Fig 1.5**)[51].

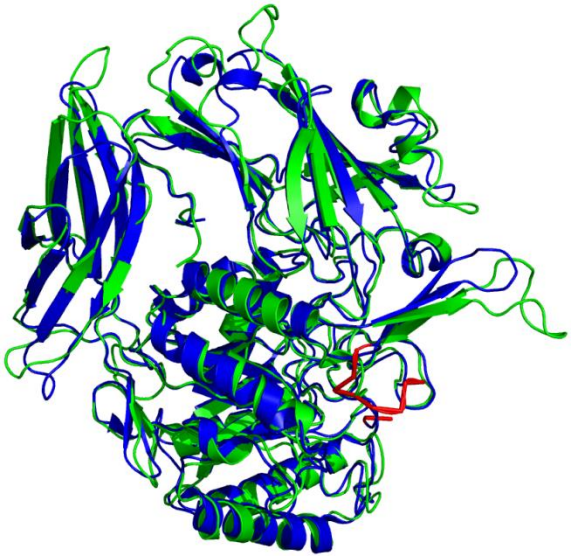

**Figure 1.4 Structural comparison of GUS**: Superposition of *E. coli* (blue, PDB 3K4D) and human GUS (green, PDB 1BHG) shows similar structures. *E. coli* GUS bacterial loop is represented in red color.

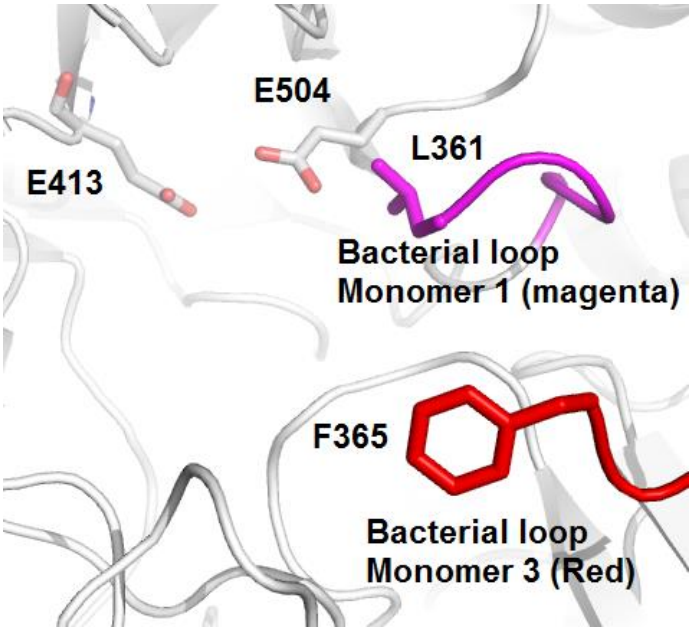


**Figure 1.5 Active site of *E. coli* GUS showing active site residues along with bacterial loop.** Bacterial loop monomer 1 is from the same monomer with the catalytic residues.

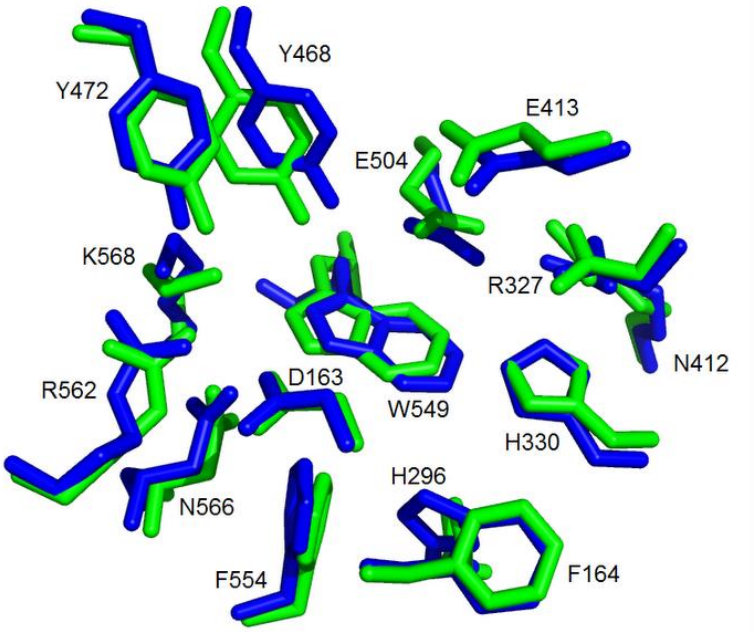


**Figure 1.6 The active site of *E. coli* (blue) and human GUS (green) are very similar and identical residue composition. Residues numbers represents the *E. coli* GUS species.**

The importance of the C6-carboxyl group of glucuronic acid was shown to interact with residues D163, Y468, E504, Y549, R562, N566, and K568; which are highly responsible for substrate recognition and binding[44]. The residues lining the active site within Human and *E. coli* GUS are identical and have very similar orientations (**Fig 1.6**).

From the structural studies of inhibitor binding to *E. coli* GUS and modeling study on Human GUS using glucuronic acid, the C-6 and C-2 β-D-glucuronide positions are highly important for determining substrate binding specificity[44, 51].

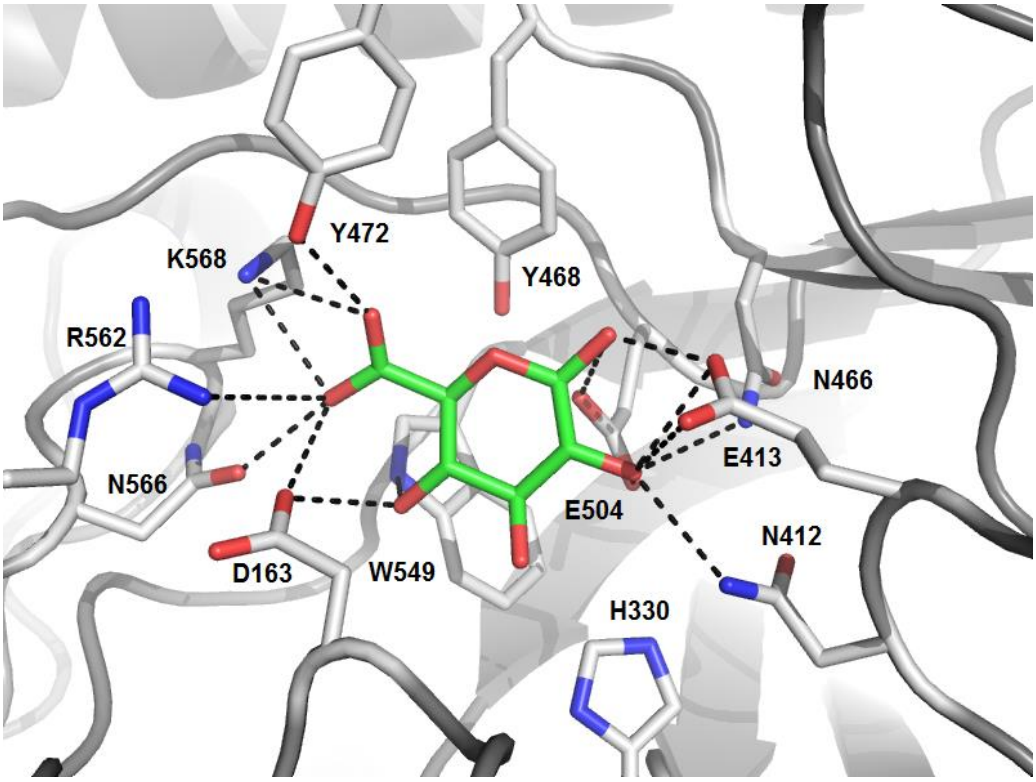


**Figure 1.7 Docked glucuronic acid (green) moiety in the active site of *E. coli* GUS (PDB: 3K4D) showing important residues responsible for recognition.** The docking studies for substrate binding were performed with GOLD Suite software package[67].

Docking studies have been performed in our laboratory by Dr. Sean Dalrymple and they reveal pose predictions with active site residues Y472, K568, R562, D163 and N566 forming hydrogen bond with C-6 carboxylate group while residues W549 and D163 form hydrogen bonds with the C-4 hydroxyl group (**Fig 1.7**). It has been proposed that positively charged residues K568 and R562 are important for stabilizing the C-6 carboxylate group through ionic contributions.

## 1.5 Hypothesis

As GUS is highly specific towards glucuronide substrates, we will use structure based design to alter the enzyme substrate specificity for accepting amide-derivatized substrate. A research study showed that the mutations in the active site have changed the substrate specificity of GUS to β-galactosidase[44]. In conjunction to this study, there are other studies that confirm that substrate specificity of GUS can be modified[68]. Further, there are two separate studies done on GUS showed that with the help of mutations optimum pH can be altered[39] and thermo stability can be improved[52] .

The implementation of structure based design to re-engineer GUS substrate specificity through point mutations for a modified substrate will result in avoiding undesirable substrate catalysis by native GUS (**Fig 1.8**).

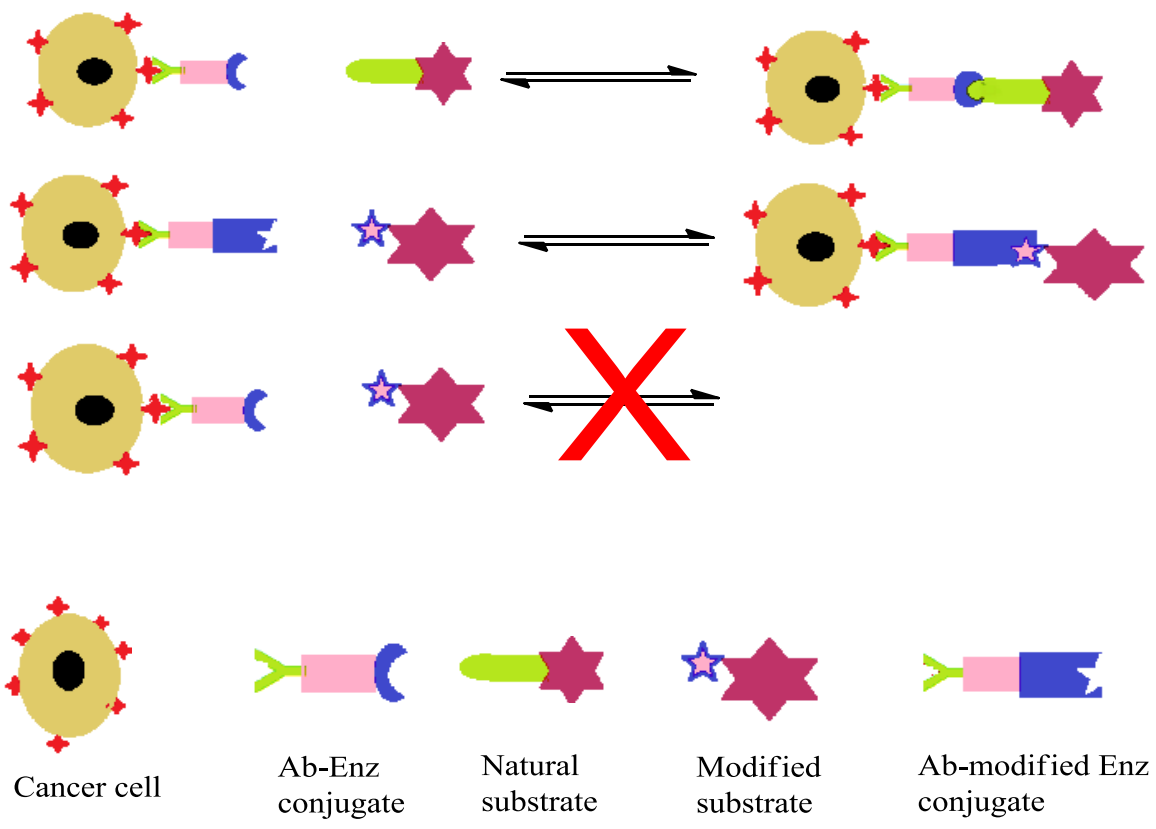


**Figure 1.8 Re-engineering of GUS based ADEPT.** (Top) Native GUS substrate selectivity, (middle) Re-engineered GUS-substrate selectivity, (bottom) Native GUS does not recognize modified substrate.

## 1.6 Research Objectives

The objectives in this research study are:

(1) Evaluate *E. coli* GUS substrate specificty towards glucuronide and glucuronamide derivatives.
(2) Re-engineering *E. coli* GUS substrate specificity through point mutations – to recover binding of glucuronamide as substrate

In order to gain insight into the substrate specificity of *E. coli* GUS and to recover activity for amide derivatized (carboxamide) substrate, mutations will be performed near the C6 carboxyl group to further explore the substrate specificity for an amide-derivatized substrate. The aim is for only the mutated version of GUS to be able to recognize the modified (amide-derivatized) substrate not the native enzyme.

We will test this modification with different aglycone moieties and kinetics will be performed to observe the changes in $k_{cat}$ and $K_m$. The best modified substrate by hypothesis would have poor or no binding (typically represented by high $K_m$ values) and very low or no turnover rate (low $k_{cat}$ values) for the native GUS and vice versa for the mutated enzyme.

The C6 carboxyl group of glucuronic acid is negatively charged and is highly important for substrate recognition. It has been proposed that utilizing this negative charge from the protein side, by making active site more negatively charged by mutations to the residues responsible for interacting with the C6 carboxyl group of glucuronic acid to block substrate recognition[44]. As a previous study showed glucuronamide is not a substrate for GUS suggesting C6 position modification to neutral carboxamide would be one way to proceed[46]. As such, it is important to obtain high quality protein which is suitably stable for the kinetic assaying procedure. Towards this goal, we attempted to optimize the currently employed protein purification procedure. Site directed mutagenesis will further explore the substrate selectivity towards synthetic substrates. These mutations will aid in further determination of residues involved in substrate recognition, specifically towards C6 carboxyl group. Efforts will be made to change substrate selectivity through point mutations, with the goal that only the mutated form of GUS will catalyze the reaction, not the wild type enzyme. Circular dichroism will be employed to study protein

secondary structures and will aid in the comparison of wild type enzyme with its mutated analogues. Isothermal titration calorimetry will be used to explore ligand binding property with both wild type and mutated enzymes. These techniques will be helpful in determining substrate binding ability with the enzyme and would be helpful in determining a better substrate. Our efforts will be optimizing the conditions for mutated enzyme to efficiently catalyze a reaction for an amide-derivatized substrate. Initial studies will be performed on *E coli* GUS as working with a bacterial strain is comparatively easier than eukaryotic strain in terms of protein expression. One of the long term goals also include changing the pH optimum of human GUS.

Ultimately once the structure based redesign approach is established, the principles will be translated to Human GUS to reduce the chance of immunogenic response for ADEPT. This will differentiate the mutated version of enzyme from the rest of endogenous enzymes. Once this mutated enzyme is in conjugation with the respective antibody, it will serve the purpose of selective drug targeting, minimizing side effects and improves the efficacy of the ADEPT system.

# 2 EXPERIMENTAL METHODS

## 2.1 Chemical Reagents

*p*-Nitrophenyl-β-D-glucuronide (PNPG), 4-methylumbelliferyl-β-D-glucuronide (MUG), and *p*-nitrophenyl-β-D-Glucopyranoside were purchased from Sigma Adlrich, Thiophenyl-β-D-Glucuronide (PGS) was obtained from Gold Biotechnology St. Louis Mo.

*p*-Nitrothiophenyl-β-D-glucuronide (PNSPG), Phenyl-β-D-glucuronide (PG), *p*-nitrophenyl-β-D-glucuronamide (PNPGun), Phenyl-β-D-glucuronamide (PGun), and 4-methylumbelliferyl-β-D-glucuronamide (MUGUN) were synthesized by Dr. Rajendra Jagdhane in laboratory of Dr. David Palmer. QAIprep Miniprep kit was purchased from QIAgen. Restriction enzyme and markers were obtained from Biolab New England and Sigma Aldrich respectively. *Pfu* DNA polymerase was purchased from Agilent. Protease inhibitor cocktail (EDTA free) was obtained from Thermo Scientific. Primers were synthesized by Alpha DNA. Other chemical reagents were of the highest quality grade purchased from Sigma-Aldrich Inc.

## 2.2 Equipment and software used in various experiments

All the kinetic measurements were performed on Varian Cary 50 - UV spectrometer while fluorescence based enzyme assays were performed on PTI fluorospectrometer. Initial docking studies were done using Gold suite software [67]. Carywin UV and Graphpad prism (Version 3.0) software were used for determining kinetic parameters. PCR reactions were performed on PTC™ 100 (Programmable thermal controller) under Program Anidko. Centrifugation was performed using Beckman Coulter Microfuge 18 and a Beckman J2-HS refrigerated centrifuge equipped with JA-25.50 rotor. For incubation and shaking, Innova 4230 refrigerated incubator/shaker was used. Cell lysis was performed using Virsonic 600 Ultrasonic Cell Disrupter. His GraviTrap™ hand columns and Superdex 200™ (gel filtration) column both from GE healthcare were used for protein purification, the later column was used with a BIO-CAD 700E, High Fast Protein Liquid Chromatography Workstation. Protein concentration was determined by NanoDrop® ND-1000 and analyzed by SDS-PAGE; Gel casting units were from

Hoefer Scientific. Barnstead NANOpure® DIamond™ (UV/UF) Ultrapure water system in all experiments. Cicular Dichroism studies were performed on PiStar-180 instrument manufactured by Applied Photophysics. CDNN deconvolution program [69] provided by Saskatchewan structural sciences centre was employed for determining spectra details. ITC experiments were performed on Nano ITC by TA Intruments Microcalorimetry. ITC data were analyzed by Nano Analyze software provided by TA instruments.

## 2.3 Plasmid Isolation, Growth and Transformation

Plasmid DNA from *E. coli* cells was isolated using QIAprep Miniprep kit protocols. The pHISTEV-GUS was prepared by Dr. Inder Sheoron (Department of Chemistry, University of Saskatchewan, Saskatoon (SK) Canada). Recombinant plasmid (10 µL) was transformed in to the DH5α competent cells (50 µL) and incubated for 30 min on ice; heat shocked for 45 s at 42˚C and then 2 min on ice. The transformation mixture was then added to 0.5 mL of LB media and incubated for 1 hour at 37˚C with shaking at 250 rpm. Cells were spun down for 3 min at 13000 rpm on the bench top centrifuge and 400 µL of the supernatant was then discarded. The cells were resuspended in remaining LB media and plated on agar plates containing kanamycin (50 µg /mL). Agar plates were incubated for 16 hrs at 37˚C. Single colonies were selected and grown in 4 ml LB media containing kanamycin (50 µg/mL). The plasmid DNA was isolated as described above and sequenced at NRC Plant Biotechnology Institute. Successful recombinant plasmids were expressed using the T7 promoter system transformed into *E. coli* BL21-gold cells.

## 2.4 Protein production and purification

A single colony containing recombinant plasmid was inoculated in 4 mL LB media containing kanamycin (50 µg/mL) and incubated at 37˚C and 250 rpm overnight. A 1 ml aliquot of the overnight culture was used to inoculate 100 mL LB containing kanamycin (50 µg/mL) which was then incubated at 37˚C, 250 rpm overnight. A 10 mL aliquot of overnight culture was used to inoculate 1L LB containing kanamycin (50 µg/mL) and incubated at 37˚C and 250 rpm. The

expression was induced with IPTG (final concentration 0.2 mM) when $OD_{600}$ reached 0.6. The cell culture was incubated at 15˚C for 15 hrs at a rotation speed of 250 rpm. The cell culture was then centrifuged in Sorvall Legend RT benchtop centrifuge at 3650 rpm for 20 min at 4˚C and the supernatant discarded. From 1L cell culture, 8 g (wet weight) cells were obtained. Cell pellets were placed in -80 ˚C for storage.

The obtained cell pellets was resuspended in 20 mL binding buffer (25 mM imidazole, 20 mM potassium phosphate, 500 mM NaCl, pH 7.4), and then lysozyme (0.5 mg/mL), DNAse (1 µg/mL), AEBSF (0.05 mg/mL) and protease inhibitor cocktail (100 µL/10 mL lysate) were added and stirred for 30 min. The sample was then sonicated for 3 min with 15s on/off intervals and the supernatant was separated from cell debris by centrifugation in Beckman J2-HS centrifuge at 15000 rpm at 4˚C for 30 min.

The supernatant was then filtered through a 0.45 µm syringe filter and 5 mL of the crude protein was loaded onto His GraviTrap™ hand columns. The column was equilibrated with 10 mL of binding buffer before loading the crude protein 5 mL (as per given protocols), washed with 10 mL of binding buffer followed by 3 x 1 mL of elution buffer (500 mM imidazole, 20 mM potassium phosphate, 500 mM NaCl, pH 7.4). One milliliter fractions were collected. The second elution was loaded onto a Superdex 200™ (gel filtration) column. The column was equilibrated with one column volume of low ionic strength buffer (20 mM HEPES, 10 mM NaCl, pH 7.4) and two column volumes of high ionic strength buffer 20 mM HEPES, 50 mM NaCl, pH 7.4 (as per given protocol, GE healthcare). The protein was run with 20 mM HEPES, 50 mM NaCl, pH 7.4 and collected 2 mL fractions at a flow rate of 1 mL/min.

## 2.5 Protein Characterization

### 2.5.1 Sodium dodecyl sulfate polyacrylamide gel electrophoresis (SDS-PAGE)

Electrophoresis was performed in sodium dodecyl sulfate containing polyacrylamide gel with known molecular weight protein marker as a control with protein samples. A 10% resolving gel and 5% stacking gel were used to characterize protein. These gels were prepared according to the recipes in **Table 2.1** and **2.2**. Protein samples were mixed with loading dye (50 mM Tris (pH

6.8), 2% SDS, 0.2% bromophenol blue (tracking dye), 20% glycerol and 1% BME (reducing agent)) and heated for 10 mins at 100˚C. Running buffer (Tris-Glycine) was poured in to the chamber followed by protein sample loaded in to the wells.

**Table 2.1 SDS-PAGE Recipe- 15 mL Separating Gel**

| Component | 10 % Gel |
|---|---|
| Water | 7.1 mL |
| 1.5 M Tris (pH 8.8) | 3.8 mL |
| 40 % Acrylamide mix | 3.8 mL |
| 10% SDS | 150 µL |
| 10% APS | 150 µL |
| TEMED | 15 µL |

**Table 2.2 SDS-PAGE Recipe- 5 mL Stacking Gel**

| Component | 5 % Gel |
|---|---|
| Water | 3.6 mL |
| 1 M Tris (pH 6.8) | 0.63 mL |
| 40 % Acrylamide mix | 0.63 mL |
| 10% SDS | 50 µL |
| 10% APS | 50 µL |
| TEMED | 5 µL |

Samples were run at 140 volts. Once sample reached the bottom of the gel, staining was perfomed using Coommasie brilliant blue. Destaining was done using fast and slow destaning solution respectively (Fast destaning solution – 30% methanol and 10% acetic acid, slow destaning solution – 50% methanol and 10% acetic acid). Gels were dried using gel drying papers (VWR) or documented by photographs.

## 2.6 Site-directed mutagenesis

Protein sequences were obtained from GenBank. Primers were designed based on the DNA sequence of the wild type *E. coli* GUS through PrimerX (www.bioinformatics.org/primerx/) via Quick change site-directed mutagenesis kit (Stratgene). Other parameters such as GC% (40 – 60%) and melting temperature (80˚C) were optimized. The plasmid DNA was isolated according to QIAprep spin miniprep kit manual protocols.

PCR reactions were performed in a final volume of 50 µL containing 5 µL of 10X PCR buffer (200 mM Tris–HCl, pH 8.8, 100 mM KCl, 100 mM $(NH_4)_2SO_4$, 20 mM $MgSO_4$, 1% Triton X-100, 1.0 mg/mL BSA); 10 ng of plasmid DNA , 1-2 µL (15 pmole) of forward and reverse primers depending upon number of base pairs (**Table 2.3**); 1 µL dNTP (10 mM), 1 µL PFu turbo DNA polymerase (2.5 U). The final volume was adjusted to 50 uL with nuclease free water. 30 µL of mineral oil was added in each of the Eppendorf tubes. Amplifications were carried out in PTC$^{TM}$ 100 (Programmable thermal controller): initial denaturation at 95$^{o}$C for 30 seconds; followed by 16 cycles of denaturation at 95$^{o}$C for 30 seconds, annealing at 55˚C for 1 min, and elongation at 68$^{o}$C for 14 min. Amplified DNA samples were digested with 1 µL of dPN1 (10 U) and incubated for an hour at 37˚C with shaking. After digestion, transformation was performed as described previously.

**Table 2.3 GUS primers for Polymerase chain reaction**

| Mutant | Primer | Primer pair (5′ → 3′) | % GC content | $T_m$ (°C) |
|---|---|---|---|---|
| K568E | Forward | CGTTGGCGGTAACAAGGAAGGGATCTTCACTCG | 54.55 | 80.6 |
| | Reverse | CGAGTGAAGATCCCTTCCTTGTTACCGCCAACG | | |
| K568Q | Forward | CGTTGGCGGTAACAAGCAAGGGATCTTCACTCG | 54.55 | 80.6 |
| | Reverse | CGAGTGAAGATCCCTTGCTTGTTACCGCCAACG | | |
| R562E | Forward | CGACCTCGCAAGGCATATTGGAAGTTGGCGGTAACAAGAAAGG | 51.16 | 79.7 |
| | Reverse | CCTTTCTTGTTACCGCCAACTTCCAATATGCCTTGCGAGGTCG | | |
| R562Q | Forward | GACCTCGCAAGGCATATTGCAAGTTGGCGGTAACAAGAAAG | 48.78 | 80.1 |
| | Reverse | CTTTCTTGTTACCGCCAACTTGCAATATGCCTTGCGAGGTC | | |
| N566D | Forward | GCATATTGCGCGTTGGCGGTGATAAGAAAGGGATCTTCACTCG | 51.16 | 79.7 |
| | Reverse | CGAGTGAAGATCCCTTTCTTATCACCGCCAACGCGCAATATGC | | |
| Y472E | Forward | GAACCGTTATTACGGATGGGAAGTCCAAAGCGGCGATTTGG | 51.22 | 78.9 |
| | Reverse | CCAAATCGCCGCTTTGGACTTCCCATCCGTAATAACGGTTC | | |
| E504Q | Forward | GCCGATTATCATCACCCAATACGGCGTGGATACG | 52.94 | 80.4 |
| | Reverse | CGTATCCACGCCGTATTGGGTGATGATAATCGGC | | |

## 2.7 Enzyme Kinetics

Both native GUS and mutants were assayed using various substrates where initial velocity of the reaction was continuously monitored by increase in absorbance over time. The cuvettes containing the protein in buffer were incubated for 5 min and the reaction was initiated by addition of the substrate. All the measurements were done in duplicate. Kinetic parameters were determined by plotting rate vs substrate concentration using Prism software. Rate of product formation was measured as change in absorbance per min following Beer's law

$$A = \varepsilon bc \quad (1)$$

where A= absorbance, Ɛ= Molar extinction coefficient, b = Optical pathlength (1 cm) and c = concentration.

All the assay preparations were kept in an ice bath while performing the assays. The enzymatic release of *p*-nitrophenol, phenol and 4-methylumbelliferone from their glucuronides and glucuronamides conjugates were monitored at 405 nm, 265 nm and 365 nm respectively. The enzyme cleavage of *p*-nitrothiophenyl-β-D-glucuronide to generate *p*-nitrothiophenol was

monitored at 408 nm. The molar extinction coefficients of *p*-nitrophenol, phenol, *p*-nitrothiophenol and 4-methylumbelliferone at pH 7.4 were 9000 $M^{-1}cm^{-1}$, 1100 $M^{-1}cm^{-1}$, 11000 $M^{-1}cm^{-1}$ and 4000 $M^{-1}cm^{-1}$ respectively. Thiophenyl-β-D-glucuronide, glucuronic acid and *p*-nitrophenyl-β-D-glucopyranoside were assayed as inhibitors against *p*-nitrophenyl-β-D-glucuronide (PNPG).

All substrate stocks were made in HEPES buffer (20 mM HEPES, 50 mM NaCl, pH 7.4) except phenyl-β-D-glucuronamide which was solubilized in 10% (v/v) DMSO, glucuronamide derivatized substrates were solubilized in a 55°C with the aid of water bath and these samples were kept at room temperature during enzymatic assays. The substrate concentration range typically varies from 0.01-1.0 mM range in an assay and all the assays were performed at room temperature (23°C ± 2).

### 2.7.1 pH optimum study

Kinetic assay were also performed at different pH values, in duplicates to determine the pH optimum for GUS activity with both PNPG and PNPGun (concentration varied over 0.01 mM – 3.0 mM). In order to cover a suitable pH range, reaction buffer was replaced with 0.1 M potassium acetate buffer (pH 4.0, 4.5, 5.0 and 5.5), 0.1M potassium phosphate buffer (pH 6.0 and 6.5), 0.1M HEPES buffer (pH 7.0, 7.5 and 8.0) and 0.1 M bicine buffer (pH 8.5 and 9.0). At each pH, release of *p*-nitrophenol was measured at 405 nm. The assays were performed using the same procedure as described above.

### 2.7.2 Data Processing

Obtained slope over time were input into the Graphpad prism (Version 3.0) software and fitted by non-linear regression to the Michaelis-Menten equation. The software output gives $V_{max}$ and $K_m$. The initial velocity data were fitted in the following equations

$$v_o = \frac{V_{max}\,S}{K_m + S} \qquad (2)$$

$$v_0 = \frac{V_{max}\,S}{[K_m(1 + (I/K_i)) + S]} \quad (3)$$

$$v_0 = \frac{V_{max}\,S}{[(1 + (I/K_i)) \,.\, (K_m + S)]} \quad (4)$$

where $V_0$ - initial velocity, $V_{max}$ - maximum velocity, [S]- substrate concentration, and $K_m$- Michaelis-Menten constant for the substrate. $K_i$ is the inhibition constant. Equation 3 and 4 represents Competitive and non-competitive inhibition models respectively.

### 2.7.3 Inhibition studies of GUS with *p*-nitrophenyl-β-D-Glucopyranoside (PNPGluc), Glucuronic acid and Thiophenyl-β-D-Glucuronide (PGS)

Assays were conducted as described above with the addition of potential inhibitors (PNPGluc or Glucuronic acid or PGS) to the reaction mixture (protein and reaction buffer) and incubated for 5 mins prior to initiation with PNPG. Three different concentrations of PNPGluc and Glucuronic acid were used (2 mM, 4 mM and 6 mM) while varying PNPG concentrations (0.01-1 mM range). In case of PGS, concentrations were (0.5 mM, 1 mM and 1.5 mM) with varying PNPG concentrations (0.01- 1 mM range). The inhibition constants for all the potential inhibitors were calculated using Sigma plot software which is discussed later in this thesis.

### 2.7.4 Fluorescence assay

The fluorescence assays were conducted with 4-methylumbelliferone as the flurophore with an excitation wavelength of 365 nm for which emissions were monitored at 445 nm. A 4-methylumbelliferone (MU) standard curve was measured to determine the rate of formation of MU- derivatized GUS substrates (**Fig 2.1**). Fluorescence assay were measured in triplicates.

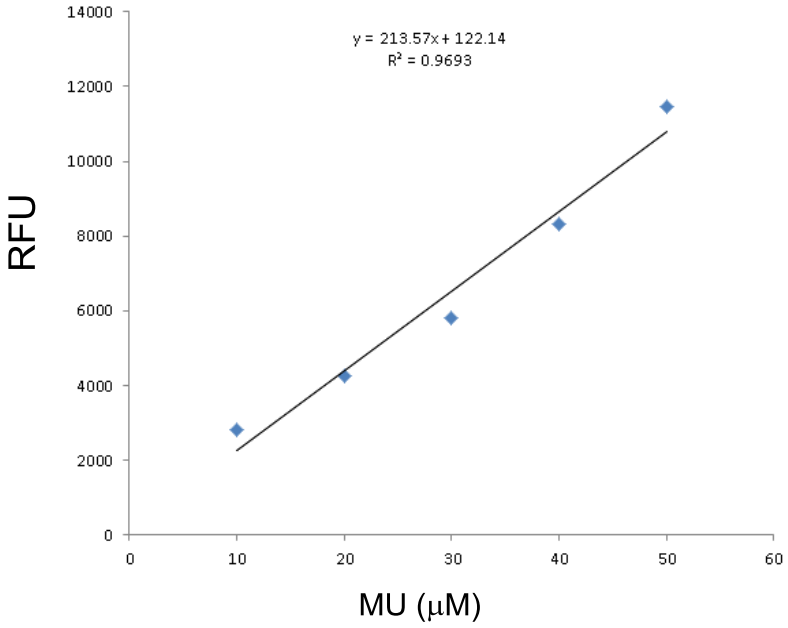


**Figure 2.1 Standard curve of 4-methylumbelliferone (MU)**

The concentration of MU produced in the assay was determined by the least squares regression equation for the line generated by the standard 4MU calibration. The equation for a line is y = mx + c, where y is the instrument reading-relative fluorescence units (RFU), x is the sample concentration (μM), m is the slope of the line, and c is the y-intercept[70].

## 2.8 Circular Dichroism Studies

CD studies on wild type and GUS mutant samples were done using 20 mM potassium phosphates buffer pH 7.4. As such protein samples were dialyzed using Vivaspin 500 (MWCO 30000 PES, 30 kDa cut-off polythersulfone membrane concentration device) protein centrifuge columns at 6000 rpm for 10 min at 4˚C using Beckman Microfuge 18 Microcentrifuge. CD measurements were performed under Far-UV region at a temperature of 4°C. CSA 4 mM ((1S)-(+)-10-camphorsulfonic acid) was used as a standard to calibrate the instrument at 290.5 nm. Five scans were conducted and averaged for each sample from 190-260 nm at 0.5 nm interval

using a 6 nm bandwidth with a rate of 5 nm per min. Samples were at a concentration of 1 mg/ml, degassed prior to the experiment and spectra were recorded for different mutants at 4˚C.

The optical path was 0.1 mm. Each spectrum was generated from the average of 5 scans. CD spectra were corrected with respect to the baseline and buffer employed for the measurement. Molar elipticity was calculated based upon the concentration of each sample using formula:

$$[\theta]=\frac{\theta\times MW\times 100}{C\times l} \quad (5)$$

Where [θ] is molar ellipticity, expressed in milidegrees $cm^2$ $decimole^{-1}$, θ is ellipticity given by the instrument (milidegrees), C is the concentration (g/mL), and $l$ is the optical length (cm). CDNN deconvolution program[69] was used in determining secondary structure details.

## 2.9 Isothermal Titration Calorimetry

GUS was dialyzed in 20 mM HEPES, 50 mM NaCl, pH 7.4 using 30 kDa cut-off polythersulfone membrane concentration device (Vivaspin) to a final concentration range of 50 - 300 µM. Samples were degassed for a period of an hour before starting the experiments. A stable baseline was achieved prior to the start of the ligand injections. Experiments were done at 25˚C and samples were stirred at rate of 300 rpm. Equilibration time between the injections was 150-200 sec. The data obtained was corrected for dilution heat by subtracting excess heat at high molar ratio of ligand to protein. Nano Analyze software provided by TA instruments was used to determine the enthalpy (ΔH), binding affinity ($K$) and entropy (ΔS) using independent model included in the software. Gibbs free energy (ΔG), $K_d$ (dissociation constant) and heat for independent model (1:1) considering one ligand per active site was determined using equation 6, 7, 8 and 9.

$$\Delta G = -RT\ln K \quad (6)$$

$$\Delta G = \Delta H - T\Delta S \quad (7)$$

$$K_d = 1/K \quad (8)$$

$$K = \frac{\ominus}{(1-\ominus)[L]} \tag{9}$$

$$L = [L] + n \ominus [P] \tag{10}$$

Combining equation 9 and 10, above gives

$$0 = \ominus^{2} - \ominus \left[1 + \frac{L}{n[P]} + \frac{1}{nK[P]}\right] + \frac{L}{n[P]} \tag{11}$$

Total heat generated from the solution in cell $V_0$ is measured as at fraction saturation $\ominus$ is

$$Q = n \ominus [P]\Delta H V_0 \tag{12}$$

By solving 11 and substituting in 12, gives

$$Q = \frac{n\,[P]\Delta H\, V_o}{2}\left[1 + \frac{L}{n[P]} + \frac{1}{nK[P]} - \sqrt{\left(1 + \frac{L}{n[P]} + \frac{1}{n\,K[P]}\right)^{2} - \frac{4L}{n[P]}}\right] \tag{13}$$

Where L AND [L] are bulk and free ligand concentration (mM)

[P] is the protein concentration in the calorimetric cell (μM)

$Q$ is the heat released/absorbed (kJ/mol), n is the stoichiometry

$K$ is the affinity constant ($M^{-1}$)

$V_o$ is the cell volume (mL) and $\Delta H$ is the enthalpy (kJ/mol).

$n$ is number of binding sites

$\ominus$ = fraction of sites occupied by ligand $L$

# 3 RESULTS AND DISCUSSION

## 3.1 Protein purification

The *E. coli* GUS-containing over-expression construct with N-terminal Histidine tag (His-tag) was successfully cloned and eexpressed previously. Full characterization of GUS and its mutants with a variety of substrates requires a purification method which produces large quantities of highly pure protein. As such, we optimized the purification to produce large quantities of purified protein to homogeneity for kinetic assays and crystallization trials. Purification of protein was carried out using a His-Gravi Trap hand column (gravity based) followed by size exclusion chromatography as reported[51]. SDS-PAGE was run to identify the purity of GUS along with reference to a known molecular weight marker. (**Fig 3.1**).The histidine tagged protein binds with nickel ions on the column. The column was then washed with binding buffer to discard the other untagged protein leaving the His-tagged protein on the column.

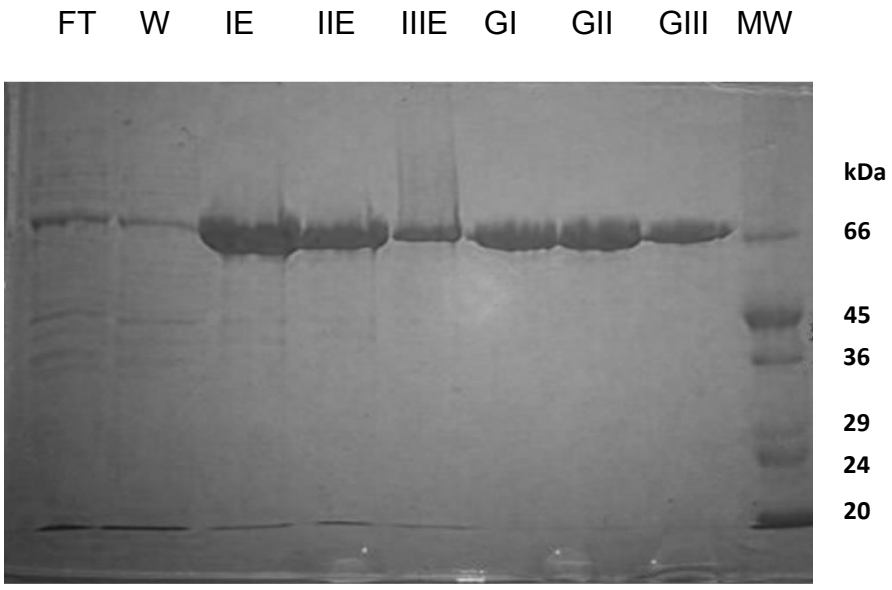


**Figure 3.1 SDS-PAGE of *E. coli* GUS** - The gel shows the purification of *E. coli* GUS from His-Gravi Trap and gel filtration column. Lanes 1: (Flow through,FT) Crude protein load onto column, Lanes 2: (Wash,W) Column wash, Lanes 3: I Elution (IE), Lanes 4: -II Elution (IIE), Lanes 5: III Elution (IIIE), Lanes 6-8: Fractions from gel filtration column (GI, GII, GIII), Lanes 9: SDS Mol. Wt. Marker (MW).

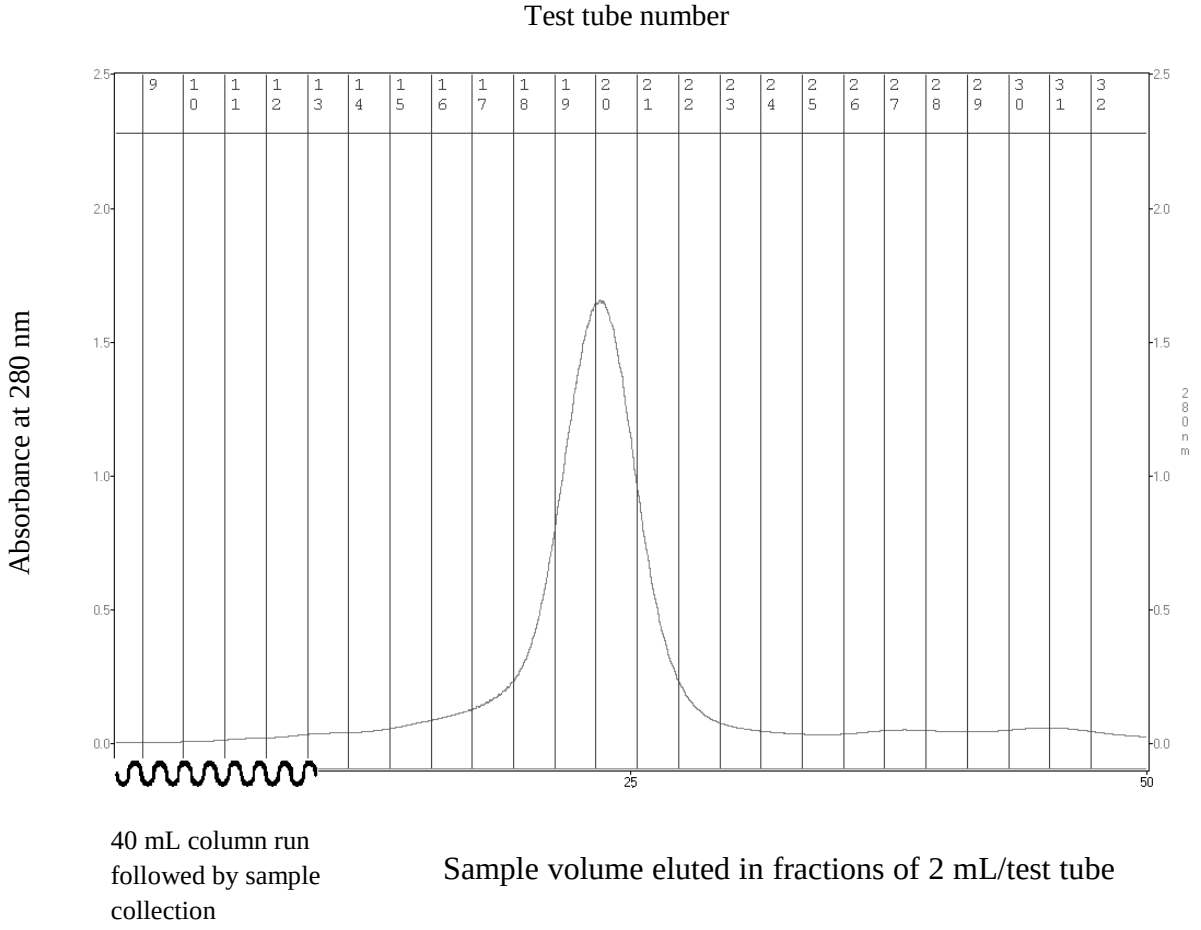


**Figure 3.2 Size exclusion chromatogram of Wt GUS**

The His-tag protein was eluted with elution buffer containing higher concentration of imidazole. As a result histidine analog imidazole competes for the binding with nickel ion on the column and the protein is eluted out with high concentration of imidazole. Eluted GUS was further purified by size exclusion/ gel fitration column. The larger molecules are excluded faster from the gel due to less volume to diffuse through the gel. While smaller molecules diffuse into the gel and migrates slowly through the column giving the pure fraction of protein. The chromatogram showing single peak represent pure fraction of protein with no contamination (**Fig 3.2**). The monomer mass of GUS is 68 kDa, which appears slightly above the 66 kDa sample of the molecular weight marker.

## 3.2 Kinetic investigation of Wt GUS Substrate specificity

GUS is a type 2 glycoside hydrolase that catalyzes the cleavage of β-D-glucuronides[43]. The enzyme is highly specific for the glucuronide moiety of the substrate. Given that glucosides are not substrates for the enzyme, the glucuronide 6-carboxylate group, with its putative negative charge, must be important for recognition of the substrate. Docking studies conducted through GOLD software with glucuronic acid showed C6 carboxylate group is important in making specific interaction with the active site residues[51]. Our docking studies showed active site residues Y472, K568, R562, D163 and N566 forms hydrogen bond with C-6 carboxylate group (as shown in **Fig 1.7**). Negatively charged C6 carboxylate group of glucuronide moeity was substituted to its neutral carboxamide, which was studied with different aglycone groups, to determine substrate selectivity of GUS. As discussed above, the carboxamide derivative BA3GNamide is not a substrate for GUS from a previous study. In order to make a poor substrate for native GUS it was tested out with different aglycone groups such as *p*-nitrophenol, phenol and 4-methylumbelliferone which were studied kinetically with glucuronide and glucuronamide derivatives. Previously it was found that any aglycone moiety can be attached to the glucuronide moiety. As a test of this, different size aglycone moieties were used. Initial velocities for the reactions were determined by straight line slope of graph, typically from the first 1 min of the reaction. The concentration of the enzyme was much smaller compared to the substrate concentration in all the assays. $V_{max}$ and $K_m$ values were obtained initially from the Prism software. The $k_{cat}$ is the substrate turnover rate by the enzyme per unit time while $k_{cat}/K_m$ value determines enzyme efficiency for the substrate.

### 3.2.1 *p*-Nitrophenyl derivatives

#### 3.2.1.1 *p*-Nitrophenyl-β-D-glucuronide (PNPG)

PNPG is a well-known substrate for Wild-type (Wt) GUS and is a widely used reporter system for gene expression[45]. When PNPG is hydrolyzed by GUS, *p*-nitrophenol (p$K_a$ = 7.1 and its molar extinction coefficient (Ɛ) is 9000 $M^{-1}cm^{-1}$) [71,72] is formed as a yellow chromogenic product. As such GUS activity was continuously monitored spectrophotometrically at 405 nm. The specificity constant for PNPG is in the order of $10^3$ $mM^{-1}cm^{-1}$, binding is 0.12 mM and the

turnover rate is 101 $s^{-1}$. One of the previous studies on Wt GUS showed 10 fold higher values for specificity while other has similar values with PNPG (**Table 3.1** and **Fig 3.3**)

(a)

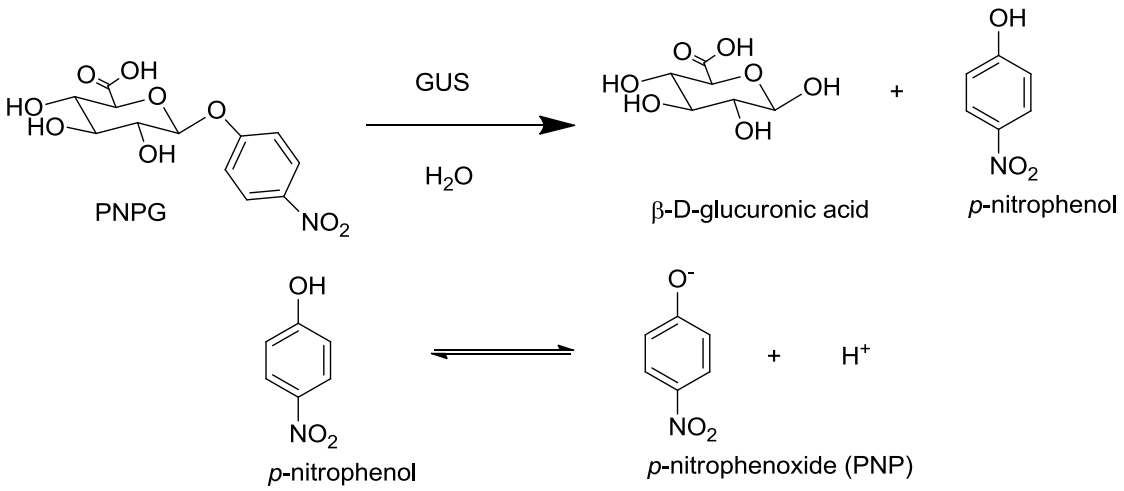


(b)

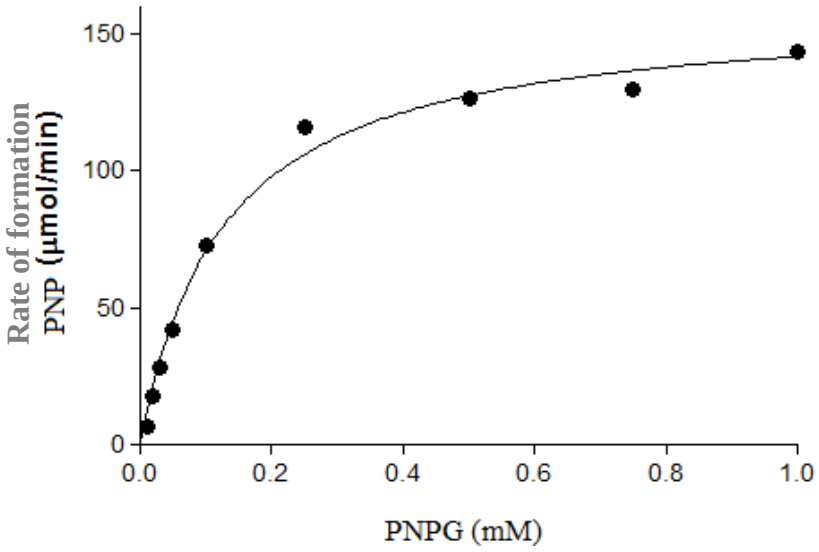


**Figure 3.3 Hydrolysis of PNPG catalyzed by Wt GUS**

(a) Reaction catalyzed by GUS using PNPG as substrate (b) Michaelis-Menten curve of Wt GUS. Measurements for each point were done in duplicate. Error bars are obscured by symbol.

**Table 3.1** Kinetic parameters of Wt GUS with its natural substrate PNPG.

| Substrate | Enzyme | $K_m$(mM) | $k_{cat}$ ($s^{-1}$) | $k_{cat}/K_m$($mM^{-1}$ $s^{-1}$) |
|---|---|---|---|---|
| **PNPG#** | ***E. coli* GUS** | **0.12 ± 0.01** | **101 ± 2** | **840 ± 73** |
| PNPG[48] | *Thermotoga maritima* GUS | 0.15 ± 0.01 | 68 ± 2 | 453 ± 33 |
| PNPG[73] | *E. coli* GUS | 0.20 ± 0.01 | 68 ± 6 | 340 ± 20 |
| PNPG[74] | *E. coli* GUS | 0.26 ± 0.01 | 109 ± 42 | 410 ± 20 |
| PNPG[75] | *E. coli* GUS | 0.24 ± 0.08 | 200 ± 6 | 833 ± 278 |
| PNPG[76] | *E. coli* GUS | 0.10 ± 0.01 | 878 ± 31 | 8600 ± 896 |

# - Bold indicates results from this study

#### 3.2.1.2 *p*-Nitrophenyl-β-D-glucuronamide (PNPGun)

PNPGun was examined as a substrate to see the effect of carboxamide versus carboxyl group at C-6 position of PNPG. The glucuronamide that is not a substrate for GUS is BA3GNamide[46]. PNPGun showed 20 fold lower turnover rate and 10 fold less substrate specificity compared to PNPG (**Table 3.2** and **Fig 3.4**). Interestingly PNPGun (0.06 mM) binds with twice the affinity of PNPG (0.12 mM). The result indicates while the amide derivative turned over at a significantly slower rate, it bound more tightly. The reason for better binding could be the inductive effect of nitro group which was not seen in phenyl and MU derivatives as discussed later in this thesis. This result would be good from a substrate point of view since there was a slower turnover rate for Wt GUS. The ideal substrate should show no turnover for the native enzyme which will ultimately aid in prevention of unwanted activation of prodrug.

(a)

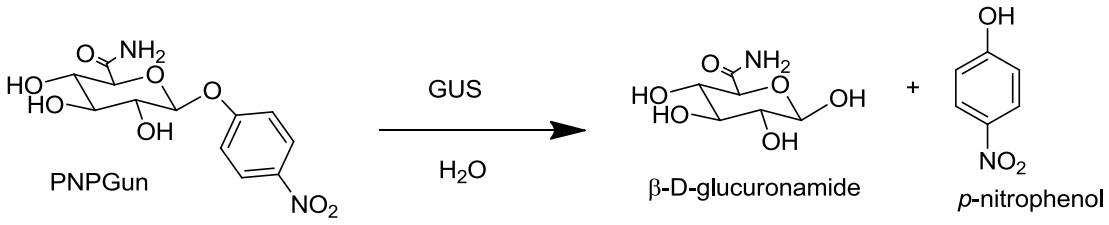


(b)

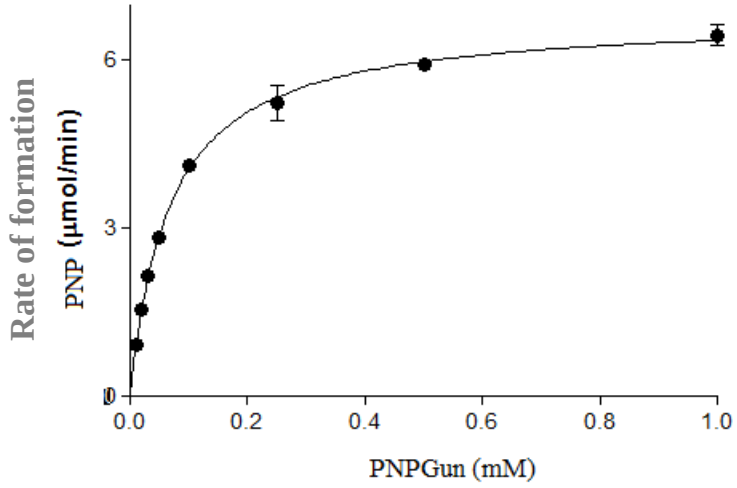


**Figure 3.4 Hydrolysis of PNPGun catalyzed by Wt GUS.**

(a) Reaction catalyzed by GUS using PNPGun as substrate (b) Michaelis-Menten curve of Wt GUS. Measurements for each point were done in duplicate. Error bars are obscured by symbol.

### 3.2.1.3 *p*-Nitrothiophenyl-β-D-glucuronide (PNSPG)

*S*-Glucuronide derivatives such as *p*-nitrothiophenyl-β-D-glucuronide (PNSPG) were also studied to determine the effect of changing substituents within the leaving group. The leaving group in this case would be *p*-nitrothiophenol (PNTP) (p$K_a$ = 4.5 )[77], which was monitored at 408 nm, has molar absorptivity (Ɛ) 11000 $M^{-1}cm^{-1}$. PNSPG was found to be a poor substrate for GUS with a turnover rate of 1000 fold less than PNPG (**Table 3.2** and **Fig 3.5**). A plausible reason could be that sulfur is less electronegative than oxygen, so it does not get protonated as fast by the general acid/ base E413 residue. As well, the size and the related conformation of PNSPG could be a reason, as atomic size of sulfur is bigger than oxygen. The results are in good

agreement with literature reports[78] which also showed 1000 fold decrease in turnover rate with *S*-glycosides (sulfur analogues) versus *O*-glycosides, although their $K_m$ values are not affected [79].

(a)

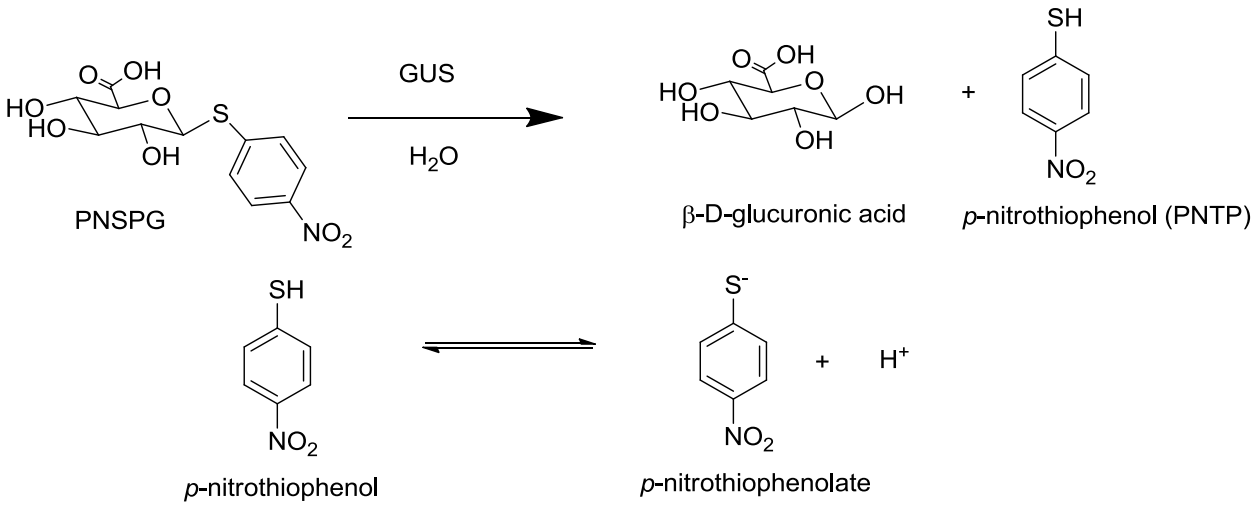


(b)

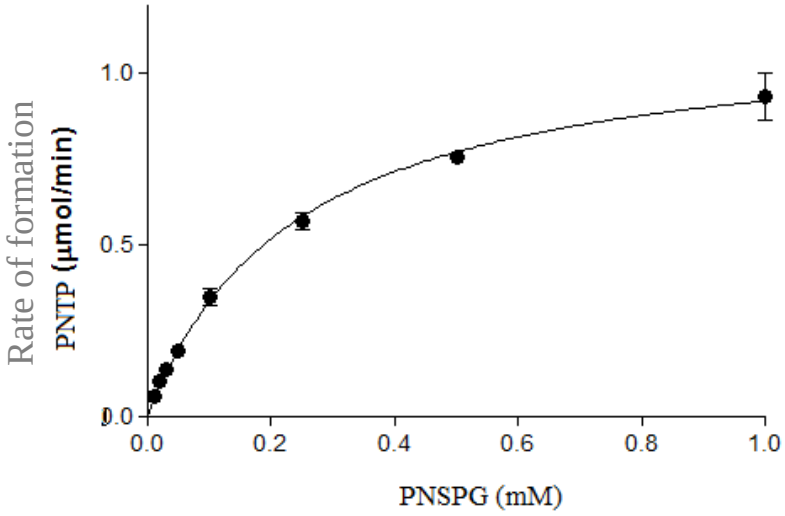


**Figure 3.5 Hydrolysis of PNSPG catalyzed by Wt GUS.**

(a) Reaction catalyzed by GUS using PNSPG as substrate (b) Michaelis-Menten curve of Wt GUS. Measurements for each point were done in duplicate. Error bars are obscured by symbol.

**Table 3.2 Kinetic parameters of *p*-nitrophenyl derivatives**.

| Substrate | $K_m$ (mM) | $k_{cat}$ ($s^{-1}$) | $k_{cat}/K_m$ ($mM^{-1}$ $s^{-1}$) |
|---|---|---|---|
| **PNPG** | **0.12 ± 0.01** | **101 ± 2** | **840 ± 73** |
| **PNPGun** | **0.067 ± 0.003** | **5.1 ± 0.1** | **86 ± 5** |
| **PNSPG** | **0.23 ± 0.02** | **(12.9 ± 0.4) x $10^{-2}$** | **(55 ± 5) x $10^{-2}$** |

# - Bold indicates results from this study

### 3.2.1.4 Inhibition of Wt GUS activity by *p*-nitrophenyl-β-D-glucopyranoside (PNPGlu)

*p*-Nitrophenyl-β-D-glucopyranoside (PNPGlu) was also studied as a substrate analogue. It differs from PNPG at C6 position by the absence of carbonyl oxygen. It showed trace activity in the presence of significantly higher concentrations of Wt GUS. As such PNPGlu is not determined to be a substrate for Wt GUS which is in agreement with previous reports in the literature[44]. Given the similarity and trace activity of PNPGlu with PNPG, it seems likely that it would be capable of fitting inside the active site. Consequently, PNPGlu was tested as an inhibitor for GUS activity with PNPG. The inhibition constant ($K_i$) is the concentration of inhibitor required to reduce the rate to half of the uninhibited value. The higher the $K_i$ value the weaker the inhibitor binds to the enzyme and *vice versa*. The $K_i$ value represents a similar concept to the $K_m$ value which is a function of ligand binding. The $K_i$ value was measured by using Sigmaplot software. Initial velocities were obtained in duplicates for each of the concentration of PNPGlu against PNPG. The obtained kinetic data was fitted to both competitive and non-competitive equations. The resulting trends shown in **Fig 3.6,** fit well to that of non-competitive inhibition model (based on value of $R^2 = 0.99$) and showed weak inhibition with $K_i$ = 5.01 mM. Significant less robust fits were obtained when the kinetic data was fitted to the equations for competitive inhibitors ($R^2 = 0.93$). The results indicate that PNPGlu binds significantly weaker than all other substrates examined in this study.

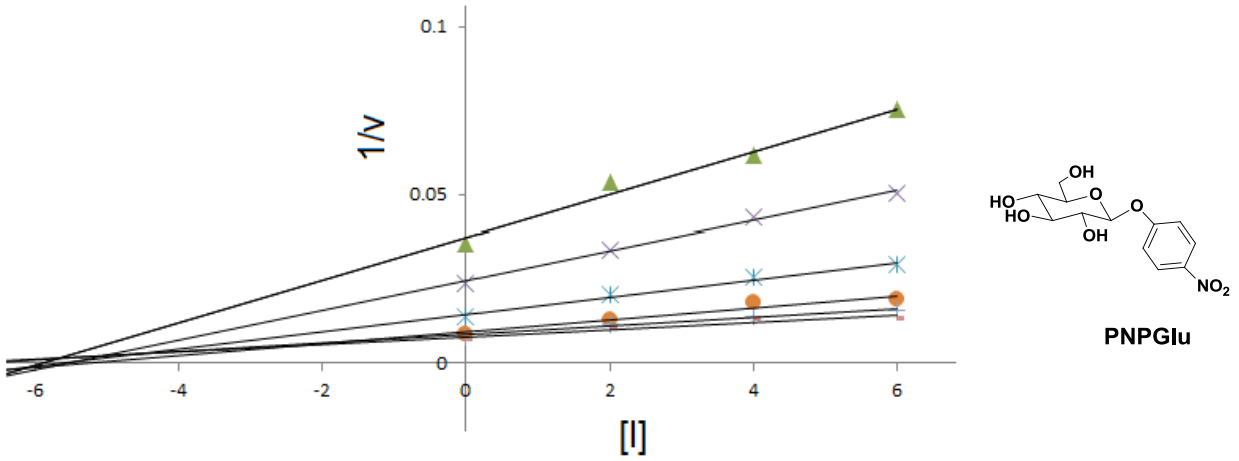


**Figure 3.6 Dixon plot of inverse initial velocity (1/μM/min) vs concentration of PNPGlu at various concentration of PNPG (range 0.01-1.0 mM).**

### 3.2.2 Phenyl derivatives

#### 3.2.2.1 Phenyl-β-D-Glucuronide (PG)

Phenyl derivatives of glucuronide and glucuronamide were also studied for substrate turnover rate and binding to examine for the un-substituted phenyl group. Kinetic results from PG showed that the turnover rate was 5 fold less and binding was 2 fold less than for PNPG ($k_{cat}$ = 22 per sec and $K_m$ = 0.23 mM) (**Table 3.3** and **Fig 3.7**). PNPG acts as a better substrate than PG due to *p*-nitrophenol (PNP) being a better leaving group (p$K_a$ = 7.1) compared to the phenol group (p$K_a$ = 9.9). The inductive effect of the nitro group in PNP plays a significant role in the level of activity[78].

(a)

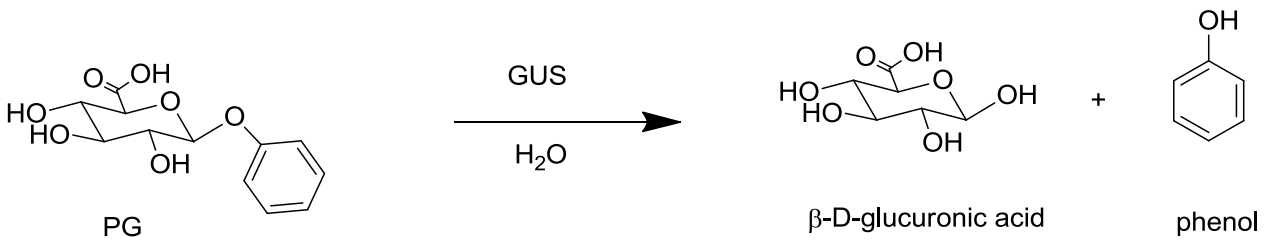

(b)

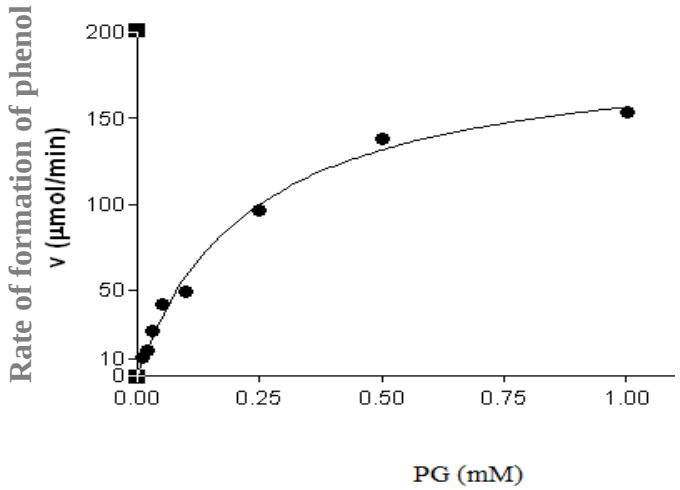


**Figure 3.7 Hydrolysis of PG catalyzed by Wt GUS.**

(a) Reaction catalyzed by GUS using PG as substrate (b) Michaelis-Menten curve of Wt GUS. Measurements for each point were done in duplicate. Error bars are obscured by symbol.

### 3.2.2.2 Phenyl-β-D-Glucuronamide (PGun)

The carboxamide analogue of the phenyl derivative namely PGun was also tested for substrate activity. Kinetic analysis of PGun exhibited 15 fold less activity than PG ($k_{cat}$ = 1.5 $s^{-1}$) with two fold weaker binding ($K_m$ = 0.41 mM) (**Table 3.3** and **Fig 3.8**). The unsubstituted phenol group is not a good leaving group and due to this PGun showed much lower activity compared to *p*-nitrophenol analogue and this may explain that the nitro group has its importance in substrate binding. Due to solubility issues with PGun in HEPES buffer, DMSO was added to reach suitable phenyl-β-D-glucuronamide solubility. In the kinetic assay with PGun substrate, the DMSO concentration was maintained at 1% for each substrate concentration.

A separate experiment was conducted to investigate the effect of DMSO on substrate binding. The enzyme was exposed to different concentrations of DMSO (1%, 5% and 10%) in final 1 mL

assay using PNPG as substrate. The $K_m$ values were found to be within the error limit when using 1% DMSO in the assay, while higher DMSO concentrations (5% and 10%) substrate binding was negatively affected (**Table 3.4**).

Acetonitrile was also examined as a solubilizing agent for PGun with the GUS kinetic assay. However, at a 1% concentration, acetonitrile was found to increase the $K_m$ value by 50% i.e. reduced the overall binding by half to its original value. Previous studies have shown the presence of either DMSO or acetonitrile negatively impact substrate binding[80].

**Table 3.3 Kinetic parameters of Phenyl derivatives**.

| Substrate | $K_m$ (mM) | $k_{cat}$ ($s^{-1}$) | $k_{cat}/K_m$ ($mM^{-1}\ s^{-1}$) |
|---|---|---|---|
| **PG** | **0.20 ± 0.02** | **22 ± 1** | **110 ± 11** |
| **PGun** | **0.41 ± 0.06** | **1.5 ± 0.1** | **3.6 ± 0.6** |

**Table 3.4 Kinetic parameters of GUS with PNPG as substarte at various concentrations of DMSO**.

| DMSO Conc. | $K_m$ (mM) | $k_{cat}$ ($s^{-1}$) | $k_{cat}/K_m$ ($mM^{-1}\ s^{-1}$) |
|---|---|---|---|
| **0%** | 0.13 ± 0.01 | 101 ± 2 | 777 ± 62 |
| **1%** | 0.14 ± 0.01 | 95 ± 2 | 679 ± 51 |
| **5%** | 0.15 ± 0.01 | 98 ± 3 | 653 ± 48 |
| **10%** | 0.19 ± 0.01 | 99 ± 3 | 521 ± 32 |

(a)

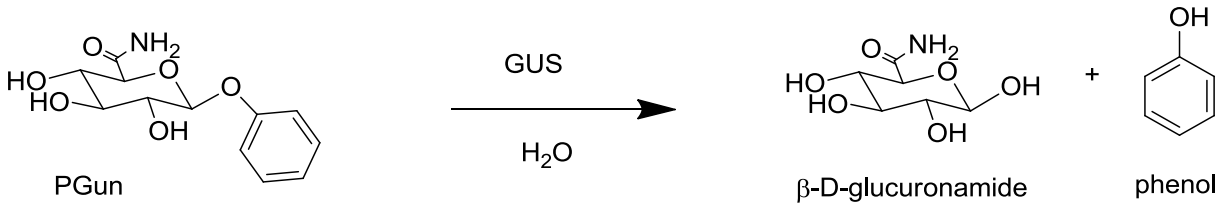


(b)

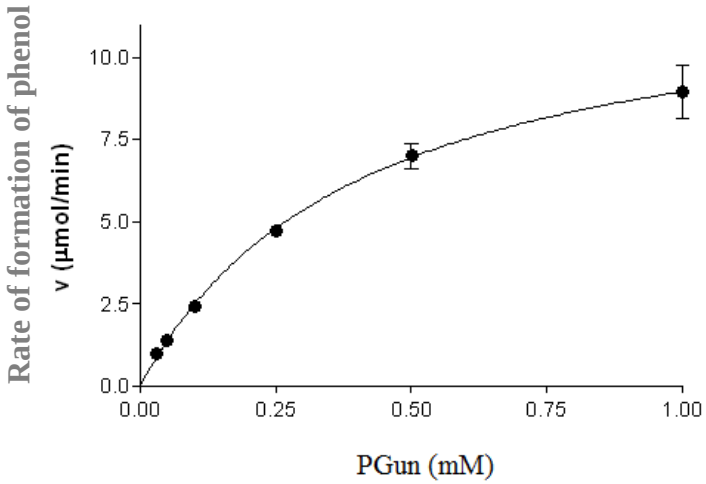


**Figure 3.8 Hydrolysis of PGun catalyzed by Wt GUS.**

(a) Reaction catalyzed by GUS using PGun as substrate (b) Michaelis-Menten curve of Wt GUS. Measurements for each point were done in duplicate. Error bars are obscured by symbol.

### 3.2.2.3 Phenyl-1-thio-β-D-Glucuronide (PGS)

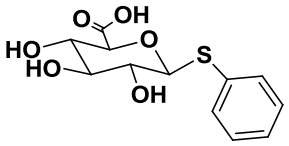


**PGS**

The *S* Glucuronide derivative PGS was studied with Wt GUS to examine the unsubstituted phenyl group. Ultimately kinetic studies revealed that PGS is neither a substrate nor an inhibitor for Wt GUS. The results are in agreement with the previous studies[78]. One study explained that thiols are not good substrates in undergoing general-acid-catalyzed nucleophilic substitution reactions at acetal centers[77, 81]. In case of *p*-nitrothiophenyl-β-D-Glucuronide (PNSPG), the nitro group of phenyl ring increases the catalytic activity compared to PGS, due to a beneficial inductive effect. Size and conformation of the PNSPG may play important role, which may partly explain why PNSPG is hydrolyzed by Wt GUS while the glucuronide of thiophenol (p$K_a$ = 6.4)[77] is not[78]. Previous studies revealed that the rate of hydrolysis is slowest for the unsubstituted phenyl group and binds weakly [45].

### 3.2.3 4-methylumbelliferyl (MU) derivatives

#### 3.2.3.1 4-methylumbelliferyl-β-D-Glucuronide (MUG)

In order to further probe the effects of the leaving group on Wt GUS activity, MUG was employed as a substrate. Additionally, the amide-derivative, namely MUGun, was also investigated for Wt GUS activity to evaluate the effects of changing the functional group at the C6 position. The cleavage product, 4-methylumbelliferone, is a fluorescencent compound, formed as a product of enzymatic catalysis of substrate MUG[82] which allowed for the kinetic assay to be evaluated using UV spectroscopy and spectrofluorometrically (**Table 3.5** and **Fig 3.9**). Experimentally results showed that MUG turnover rate ($k_{cat}$) is 43 $s^{-1}$ and $K_m$ = 0.11 mM,

was the same as PNPG. Two separate studies, one using human GUS and the other using *E. coli* GUS used MUG as substrate and showed specificity at the same scale (~100 $mM^{-1}S^{-1}$). Using different leaving groups like *p*-nitrophenol, phenol, 4-methylumbelliferone suggests that the nitro group has a significant effect on substrate catalysis rate.

(a)

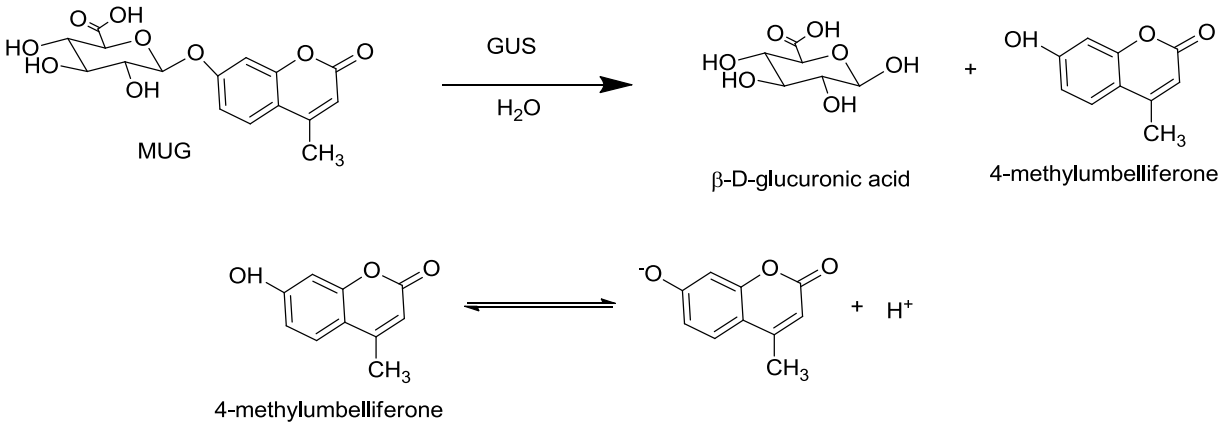


(b)

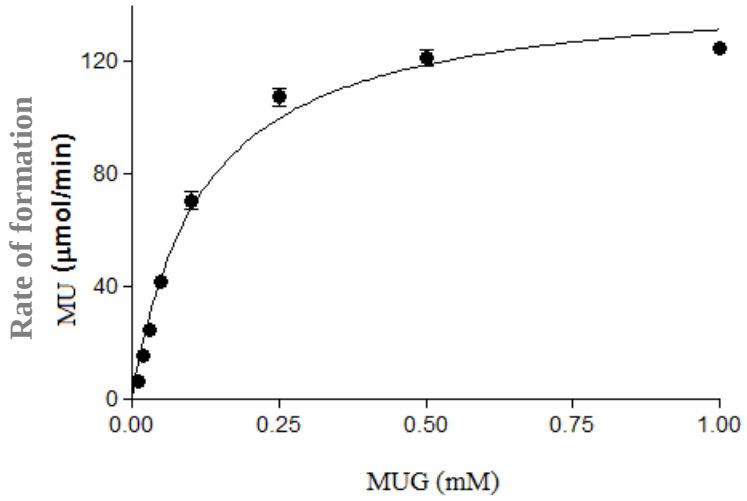


**Figure 3.9 Hydrolysis of MUG catalyzed by Wt GUS.**

(a) Reaction catalyzed by GUS using MUG as substrate (b) Michaelis-Menten curve of Wt GUS. Measurements for each point were done in duplicate. Error bars are obscured by symbol.

### 3.2.3.2 4-methylumbelliferyl-β-D-Glucuronamide (MUGun)

Kinetic assays performed with the amide-derivative, namely MUGun, revealed two fold weaker binding ($K_m$ = 0.20 mM) than MUG while the turnover rate was 9 fold slower than MUG ($k_{cat}$ = 5 $s^{-1}$). Kinetic parameters were determined on both by UV spectroscopy and spectrofluorometrically (**Table 3.5** and **Fig 3.10**). The slower turnover and weaker binding observed for the MUGun is consistent with the kinetic findings for the PG/PGun substrate pair. Interestingly, while a similar reduction in the turnover rate was observed for the PNPG/PNPGun pair, the binding in that case was found to be tighter for the amide analogue.

(a)

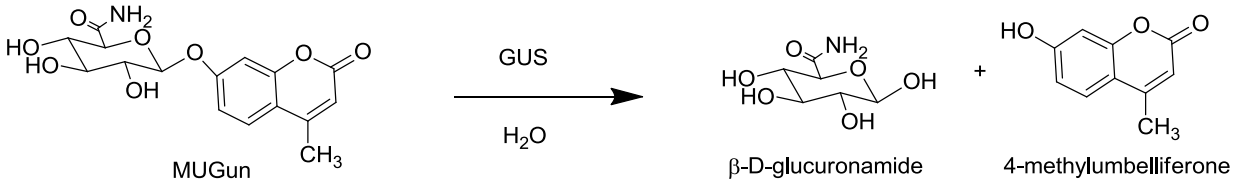


(b)

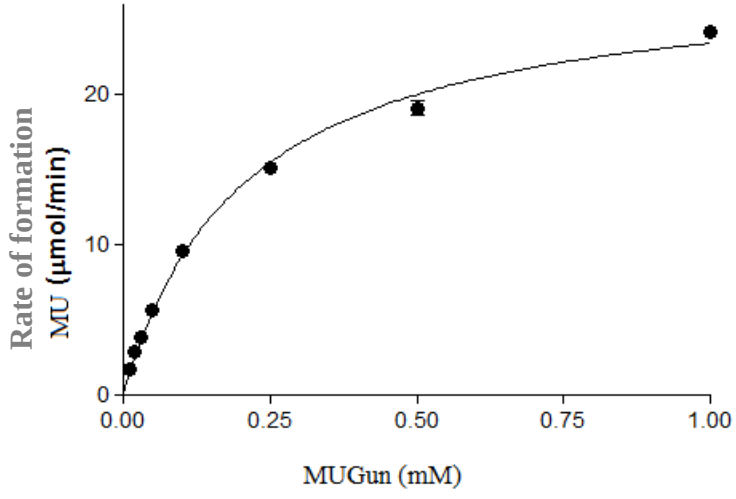


**Figure 3.10 Hydrolysis of MUGun catalyzed by Wt GUS.**

(a) Reaction catalyzed by GUS using MUGun as substrate (b) Michaelis-Menten curve of Wt GUS. Measurements for each point were done in duplicate. Error bars are obscured by symbol.

**Table 3.5 Kinetic parameters for MUG and MUGun. (F)-spectrofluorometrically, (UV)-ultravoilet**.

| Substrate | $K_m$ (mM) | $k_{cat}$ ($s^{-1}$) | $k_{cat}/K_m$ ($mM^{-1}s^{-1}$) |
|---|---|---|---|
| **MUG (UV)** | **0.11 ± 0.01** | **47 ± 1** | **390 ± 44** |
| MUG[47] | 2.76 | 276 | 100 |
| MUG[51] | n/a | n/a | 134 ± 12 |
| **MUGun (UV)** | **0.20 ± 0.06** | **5 ± 1** | **25 ± 5** |
| **MUG (F)** | **0.11 ± 0.02** | **43 ± 3** | **391± 77** |
| **MUGun (F)** | **0.25 ± 0.1** | **6 ± 1** | **25 ± 10** |

**Table 3.6 Summary of kinetic parameters of various substrates used against Wt GUS**

| Substrate | $K_m$ (mM) | $k_{cat}$ ($s^{-1}$) | $k_{cat}/K_m$ ($mM^{-1}s^{-1}$) |
|---|---|---|---|
| **PNPG** | **0.12 ± 0.01** | **101 ± 2** | **840 ± 73** |
| **PNPGun** | **0.067 ± 0.003** | **5.1 ± 0.1** | **86 ± 5** |
| **PNSPG** | **0.23 ± 0.02** | **(12.9 ± 0.4) x $10^{-2}$** | **(55 ± 5) x $10^{-2}$** |
| **PGS** | **n/a** | **n/a** | **n/a** |
| **PG** | **0.20 ± 0.02** | **22 ± 1** | **110 ± 11** |
| **PGun** | **0.41 ± 0.06** | **1.5 ± 0.1** | **3.6 ± 0.6** |
| **MUG** | **0.11 ± 0.01** | **47 ± 1** | **390 ± 44** |
| **MUGun** | **0.20 ± 0.06** | **5 ± 1** | **25 ± 5** |
| **MUG (F)** | **0.11 ± 0.02** | **43 ± 3** | **391± 77** |
| **MUGun (F)** | **0.25 ± 0.1** | **6 ± 1** | **25 ± 10** |
| **PNPGluc** | **trace activity, $K_i$ = 5 mM** | | |

*****n/a- PGS was neither a substrate nor an inhibitor

## 3.3 Kinetic Investigation of GUS Mutants

Site directed mutagenesis was performed on residues which were believed to be important for binding substrate within the active site. As crystallographic evidence for substrate binding is not available, docking studies were used to initially identify which residues could be potentially important targets. In addition to elucidating putative roles for substrate binding, the mutagenic GUS study was also aimed at improving the catalytic activity of the PNPGun substrate in the context of ADEPT specificity. As a result only mutated analogs of GUS will catalyze the reaction for amide-derivatized substrate not the native GUS. In this case PNPGun was used initially to optimize the mutations for GUS.

The enzymatic catalysis takes place through residues E504 and E413, which are within 3 Å of the glycosidic bond oxygen[44]. E504 acts as a nucleophile, while E413 acts as general acid/base. The N terminal 180 residues represents the sugar binding domain of family 2 glycosyl hydrolases[66], whereas the C terminal domain (residues 274-603) forms an $(\beta/\alpha)_8$ barrel and contains the active-site residues[50, 66]. Residues Y472, E504, R562, N566 and K568 are present on C terminal domain making important interactions with the substrate as per docking studies (**Fig 1.7**) and they all line the substrate binding pocket[44, 51, 67].

Preliminary modeling studies showed that both PNPG and PNPGun interact with the active site residues in a similar manner (**Fig 3.11**). Interestingly, kinetic experiments on Wt GUS revealed PNPGun has a significantly reduced turnover rate although the binding was twice as strong. In order to recover the activity for PNPGun which would make it a better substrate for use in ADEPT, point mutations were made to the residues proposed to make important interactions with the derivatized C6 position. The point mutations were chosen specifically to also probe which residues were important for native substrate binding.

From our hypothesis, it was also suggested that the positively-charged residues lysine 568 and arginine 562 interact with the negatively charged C6 carboxylate of PNPG when bound to the enzyme. To test this hypothesis, site-directed mutants were generated, and activity of these mutants was compared to the wild-type enzyme using a glucuronide derivative (PNPG) and its neutral glucuronamide analouge (PNPGun).

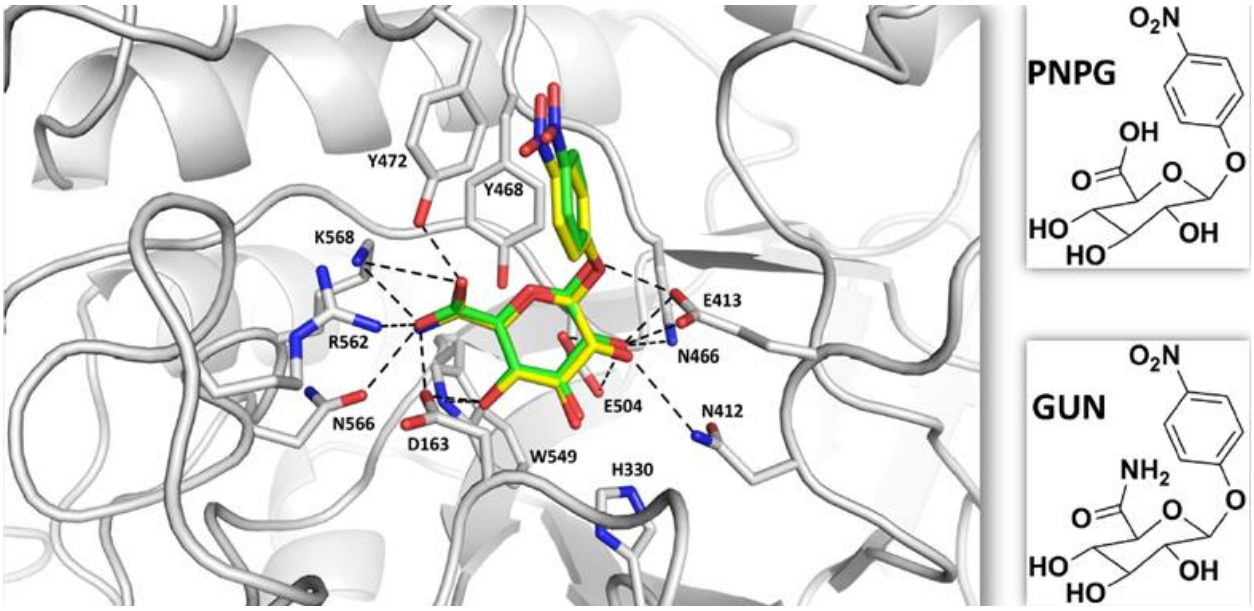


**Figure 3.11 PNPG and PNPGun are modeled in the active site of *E. coli* GUS (PDB: 3K4D). PNPG (green) and PNPGun (yellow)**

To examine the hypothesis, positively charged residues were mutated to negatively charged or neutral residues to investigate the ionic interactions. The residues forming the binding pocket as per docking studies were mutated. The resultant mutants were aimed considering the C6 carboxylate interaction with the native GUS residues. Successful mutations were made to Y472E, E504Q, R562E, N566D, K568E and K568Q. The mutants were purified with minimal impurities which were verified by SDS-PAGE (**Fig 3.12**).

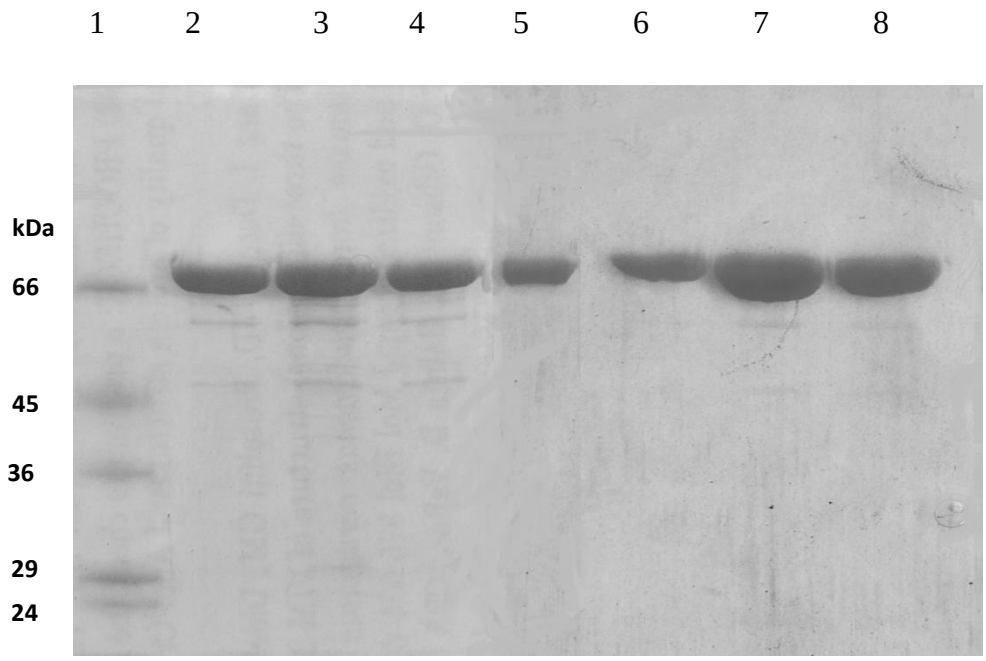


**Figure 3.12 SDS-PAGE of GUS mutants.**
From left, Lane 1: SDS Marker. Lane 2: R562E. Lane 3: R562Q. Lane 4: K568E. Lane 5: K568Q. Lane 6: Y472E. Lane 7: N566D. Lane 8: E504Q.

### 3.3.1 E504Q

E504 is an important residue in active site for enzymatic catalysis, acting as catalytic nucleophile. It attacks at the anomeric carbon (C1) of the glucuronic acid moiety which leads to the formation of glycosyl enzyme intermediate (**Scheme 2**). The docking studies revealed E504 forms hydrogen bonds with the C2 hydroxyl group. Glutamic acid at this position was mutated to glutamine, which removed the charge and kept the size constant. This mutation should allow for the stabilizing hydrogen bond to form with the substrate while eliminating the role as nucleophile. As such, it was expected that this mutant would not exhibit significant activity. Indeed E504Q mutation results in marginal 0.01 % activity (**Table 3.7** and **Fig 3.13**), which is consistent from previous results (**Table 3.9**). As well no activity was observed for PNPGun (**Table 3.8**), which further supports the fundamental role played by E504 in enzymatic catalysis.

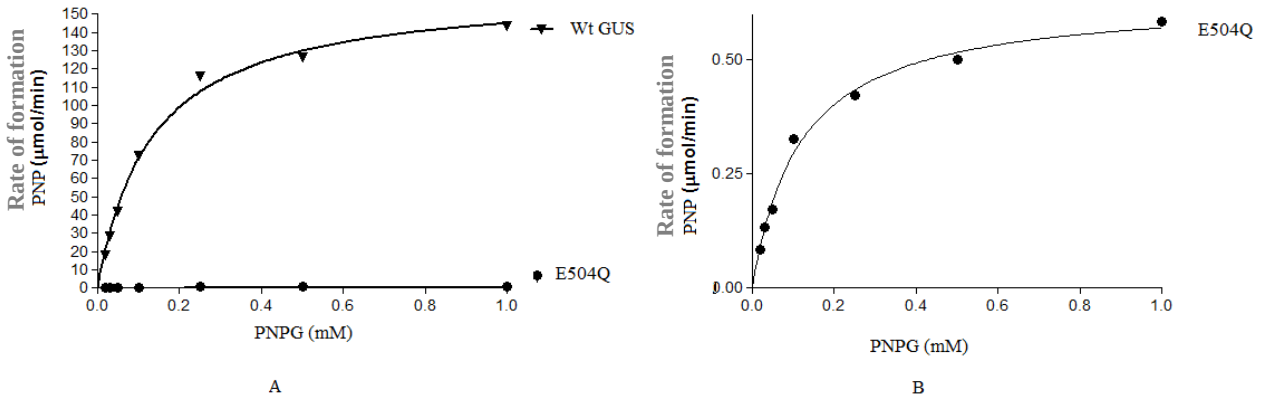


**Figure 3.13 Hydrolysis of PNPG catalyzed by GUS E504Q**.

(A) Michaelis-Menten curve comparison of Wt GUS and GUS E504Q using PNPG as substrate. (B) Michaelis-Menten curve of GUS E504Q. Measurements for each point were done in duplicate. Error bars are obscured by symbol.

### 3.3.2 R562Q/ R562E

R562 is believed to be important for substrate binding as docking studies suggests a strong interaction with the C6 carboxyl group of PNPG. Arginine is presumed to have a stabilizing effect through ionic interaction with the negatively charged C6 carboxylate. Mutating arginine to the neutral charged glutamine (R562Q) greatly reduced the activity to 1.5 % of the wild type activity for both PNPG (**Table 3.7** and **Fig 3.14)** and PNPGun (**Table 3.8** and **Fig 3.15**) while substrate binding ($K_m$) was not effected compared to the wild type.

R562 was also mutated to glutamate (R562E) to introduce the negative charge which would hinder the formation of hydrogen bonding to C6 carboxylate of the PNPG. However kinetic results showed similar binding to that of wild type GUS with significant reduced activity (0.03%) (**Table 3.7** and **Fig 3.16**). This would suggest in this case that ionic contributions are not essential for binding per se, but are required for functional binding. In the context of the previous experiment, the R562E mutation was not expected to have as significant an impact on the activity with the neutral C6 amide of PNPGun. However, the kinetic analysis showed trace activity for R562E with PNPGun which could not be quantified (**Table 3.8**). Another

explanation for decreased activity of the R562E mutant could be difference in size between the residues. A smaller residue in this position could interrupt the steric fit for productive substrate binding. Lastly, the anticipated effect of introducing a negative charge at R562 may have been partially offset by the presence of an adjacent positively charged residue, namely K568.

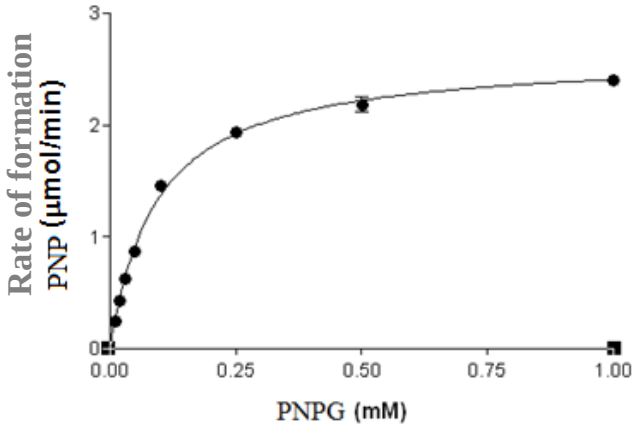


**Figure 3.14 Hydrolysis of PNPG catalyzed by R562Q.**

Michaelis-Menten curve of R562Q. Measurements for each point were done in duplicate. Error bars are obscured by symbol.

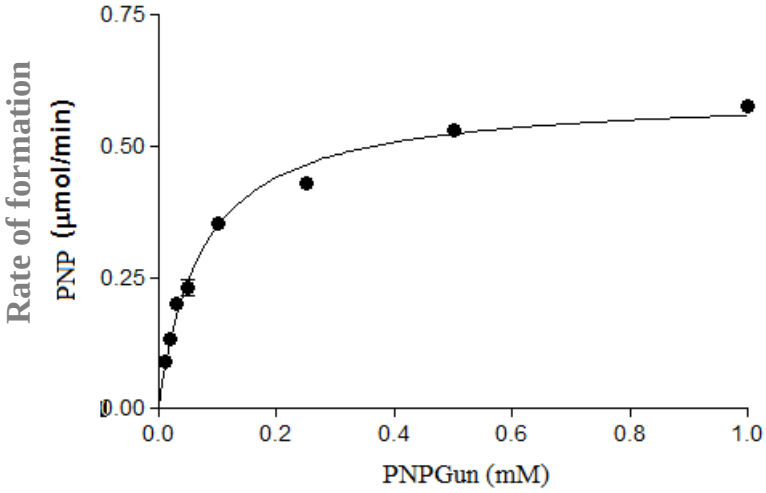


**Figure 3.15 Hydrolysis of PNPGun catalyzed by R562Q.**

Michaelis-Menten curve of R562Q. Measurements for each point were done in duplicate. Error bars are obscured by symbol.

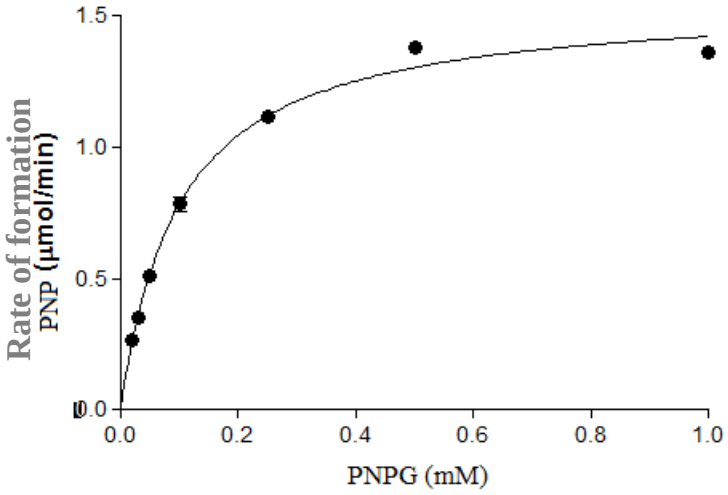


**Figure 3.16 Hydrolysis of PNPG catalyzed by R562E.**

Michaelis-Menten curve of R562E. Measurements for each point were done in duplicate. Error bars are obscured by symbol.

### 3.3.3 K568Q/K568E

In addition to R562, K568 also provides a positively charged hydrogen bonding group for interaction with the C6 carboxylate of PNPG. Within this region, the active site can be made less positively charged by replacing the lysine with a neutral glutamine residue (K568Q) or with a negatively charged glutamate (K568E). Both of these mutants were produced, purified, and characterized through kinetics to establish their effect on PNPG and PNPGun activity.

The kinetic data shows that mutation of K568 to either glutamine or glutamate results in an enzyme with complete loss of activity for both PNPG and PNPGun . The results indicate that this residue is vitally important for catalytic activity. These deleterious mutations are in line with previous conducted studies[44] (**Table 3.9**). Although the kinetic data shows K568 is vital for assisting substrate turnover; it is unclear as to whether the substrate is binding in the active site as K568 was found, through modelling studies, to be a potentially important residue for stabilizing binding of the functional group at the C6 position of the substrate. In order to obtain

such information, Isothermal titration calorimetry (ITC) was performed on this GUS mutant and will be discussed below.

### 3.3.4 Y472E

Tyrosine 472 was found, through modelling studies to be a potentially important residue for stabilizing binding of the functional group at the C6 position of the substrate. Y472 is one of three tyrosine residues (Y469 and Y468) which are part of an adjacent loop postulated to play a role in binding the sugar portion of the substrate as well as stabilizing the aglycone moiety [51, 61].

It was anticipated that the Y472E mutant would disrupt hydrogen bond formation with the C6 carboxylate of PNPG due to charge-charge repulsion. As with previous mutants in this region, interaction of a negatively charged proton acceptor residue with the amide functionality of PNPGun was expected to enhance binding and potentially increase substrate reactivity. The kinetic data revealed the Y472E mutation results in weaker binding and decreased PNPG activity. The results suggests that the tyrosine residue is responsible for the proper steric fit of the substrate in the active site (**Table 3.7** and **Fig 3.17**) and PNPGun activity was not observed (**Table 3.8**). The previous studies on GUS obtained from different organisms showed reduced activity when mutating these tyrosines (**Table 3.9)**. In case of *Scutellaria baicalensis* GUS Y281A mutation reduced the activity to 0.1%, while Y504A mutation in Human GUS showed 0.07 % activity. Similarly in *Acidobacterium capsulatum* GUS, Y334F and Y243A mutations showed activity by less than 1% (**Table 3.9)**.

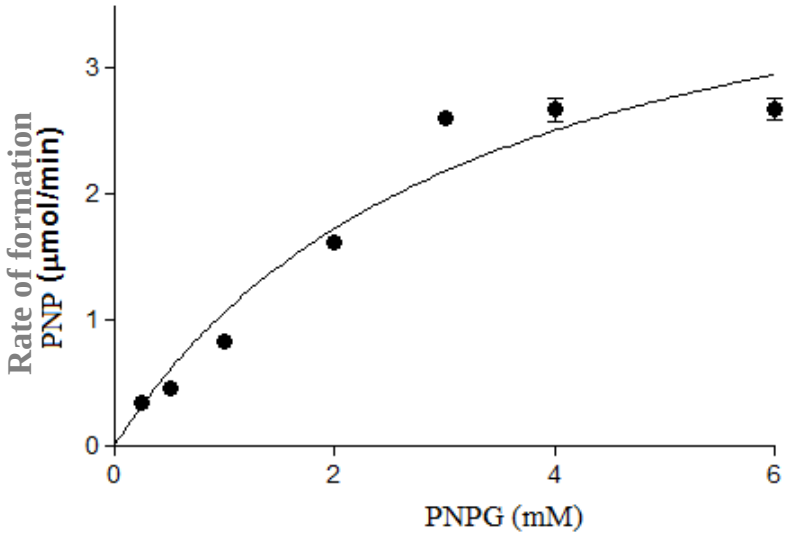


**Figure 3.17 Hydrolysis of PNPG catalyzed by Y472E.**

Michaelis-Menten curve of Y472E. Measurements for each point were done in duplicate. Error bars are obscured by symbol.

### 3.3.5 N566D

Modelling studies on glucuronic acid, PNPG, and PNPGun all suggest hydrogen bonding interactions are in operation between N566 and the functional groups (carboxylate and amide) at the C6 position. As with previous mutants, N566D was anticipated to experience repulsion with the carboxylate at the C6 position of PNPG while participating in stabilizing ionic interaction with C6 amide group of the PNPGun. While this mutation results in loss of activity of the enzyme and 10 fold decrease in binding with PNPG (**Table 3.7** and **Fig 3.18**), no activity was seen with PNPGun (**Table 3.8**). A study using *E. coli* GUS, where N566 was mutated to serine (N566S), resulted in a decrease of activity to 4%[74] (**Table 3.9**) while in this study N566D results in marginal activity (0.04 %). The plausible reason for N566D mutation is that it would remove the potential for the residue to act as a hydrogen bond donor, which is likely the cause of reduced binding and inability to help stabilize the substrate in a productive binding mode. In the case of PNPGun, it seems that the ionic portion of the interaction is not as important as there being the correct hydrogen bond donor present on the residue. The obtained result suggests importance of this residue at its position.

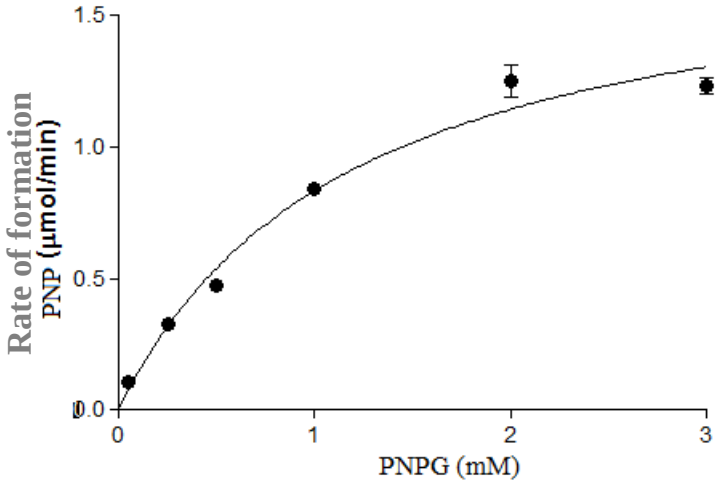


**Figure 3.18 Hydrolysis of PNPG catalyzed by N566D.**

Michaelis-Menten curve of N566D. Measurements for each point were done in duplicate. Error bars are obscured by symbol.

**Table 3.7 Kinetic parameters of GUS mutants towards PNPG.**

| Enzyme | Substrate | $K_m$ (mM) | $k_{cat}$ ($s^{-1}$) | $k_{cat}/K_m$ ($mM^{-1}s^{-1}$) | % Activity |
|---|---|---|---|---|---|
| Wt GUS | PNPG | 0.12 ± 0.01 | 101 ± 2 | 840 ± 73 | 100 |
| N566D | PNPG | 1.2 ± 0.2 | (40 ± 3) x $10^{-3}$ | (34 ± 6) x $10^{-3}$ | 0.04 |
| Y472E | PNPG | 3.2 ± 0.9 | (10 ± 1) x $10^{-2}$ | (3 ± 1) x $10^{-2}$ | 0.1 |
| E504Q | PNPG | 0.11 ± 0.01 | (14 ± 1 ) x $10^{-3}$ | 0.11 ± 0.01 | 0.01 |
| R562E | PNPG | 0.10 ± 0.01 | (35 ± 1) x $10^{-3}$ | (36 ± 2) x $10^{-2}$ | 0.03 |
| R562Q | PNPG | 0.09 ± 0.01 | 1.66 ± 0.01 | 18 ± 1 | 2 |
| K568Q | PNPG | No activity | | | n/a |
| K568E | PNPG | No activity | | | n/a |

**Table 3.8 Kinetic parameters of GUS mutants towards PNPGun.**

| Enzyme | Substrate | $K_m$ (mM) | $k_{cat}$ ($s^{-1}$) | $k_{cat}/K_m$ ($mM^{-1}s^{-1}$) | % Activity |
|---|---|---|---|---|---|
| Wt GUS | PNPGun | 0.067 ± 0.003 | 5.1 ± 0.1 | 86 ± 5 | 100 |
| K568Q | PNPGun | No activity | | | n/a |
| K568E | PNPGun | No activity | | | n/a |
| E504Q | PNPGun | No activity | | | n/a |
| R562Q | PNPGun | 0.07 ± 0.01 | (68 ± 1) x $10^{-3}$ | (97 ± 5) x $10^{-2}$ | 1 |
| R562E | PNPGun | No activity | | | n/a |
| Y472E | PNPGun | No activity | | | n/a |
| N566D | PNPGun | No activity | | | n/a |

**Table 3.9 Comparison of the percent activity of GUS mutants with previous published results**

| C-terminal Residues | ***E. coli* GUS (%)** | *Scutellaria baicalensis* GUS[83] % | *E. coli* GUS[74] (%) | Human GUS[47] (%) | *Acidobacterium capsulatum* GUS[49] (%) |
|---|---|---|---|---|---|
| **Catalytic residues** Glutamates (E) | **E504Q 0.01** | E212A 0.02<br>E329A 0.001 | | E540A 0.001<br>E451A 0.005 | E287G 0.01<br>E173G 0.02<br>E173A 0.01 |
| **Sugar Binding Residues** | **Y472E 0.1**<br>**N566D 0.04**<br>**R562E 0.03**<br>**R562Q 2**<br>**K568E 0**<br>**K568Q 0** | Y281A 0.1 | N566S 4<br><br><br>K568Q 0 | Y504A 0.07 | Y334F 0.5<br>Y243A 0.02<br>Y219A 44 |

The experimental results show that mutations lead to loss of activity of enzyme for both PNPG and PNPGun. Our studies suggest further mutational studies need to be performed to further probe the residues in reactivation of PNPGun as a better substrate. Directed evolution experiments with random mutagenesis could be an approach that can be applied[39, 44, 68]. There is a further need of finding appropriate mutations required to make PNPGun a good substrate.

## 3.4 pH and Temperature study

The optimal pH for the activity of Wt GUS was determined by assaying at different pH levels using both substrates PNPG and PNPGun. From an ADEPT point of view, enzyme should undergo efficient catalysis at physiological pH (pH = 7.4) for catalyzing the reaction. The pH study was performed to analyze the enzyme catalysis rate for amide-derivatized substrates. Temperature study was also performed to investigate enzyme stability at different temperatures.

### 3.4.1 pH optimum study of Wt GUS

The optimal pH of the Wt GUS was determined at room temperature (24°C) over a pH range of 4-9 at every half interval. Kinetic parameters $V_{max}$ and $K_m$ were determined at each interval and the data was measured in duplicate. The enzyme (Wt GUS) was found to be most active in pH range 7-8 (**Fig 3.19**) which was consistent with the previously obtained results using PNPG as substrate[52, 68].

(A) (B)

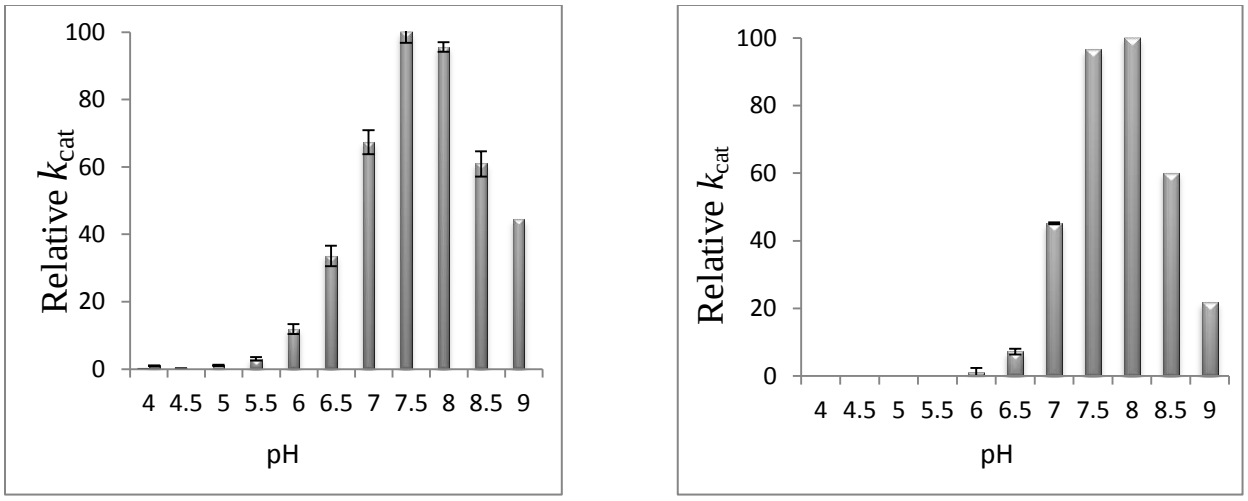


**Figure 3.19 Relative activities ($k_{cat}$) of Wt GUS at various pHs**.

Kinetic assays were performed at room temperature. (A) Activity profile with PNPG as substrate over the concentration range 0.01 – 3.0 mM. (B) Activity profile with PNPGun as substrate over the concentration range 0.01 – 1.0 mM.

From the kinetic assays performed at various pH levels, it was found that $K_m$ values for PNPGun ranged from 0.03-0.08 mM, while $K_m$ for PNPG varied from 0.16-1.0 mM.

(A) (B)

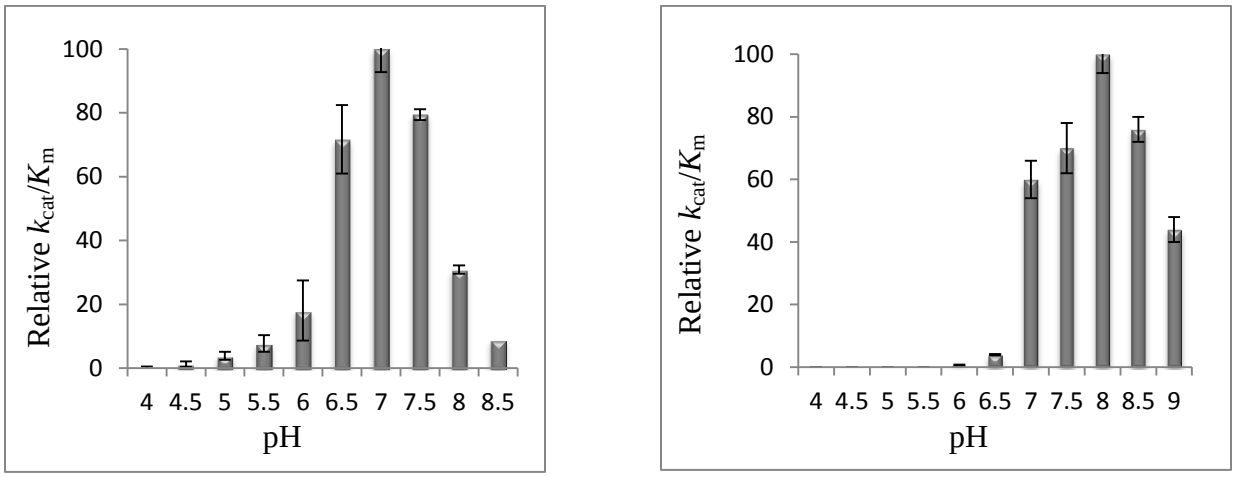


**Figure 3.20 Relative $k_{cat}/K_m$ of Wt GUS at various pHs.**

Kinetic assays were performed at room temperature. (A) Relative $k_{cat}/K_m$ profile with PNPG as substrate. (B) Relative $k_{cat}/K_m$ profile with PNPGun as substrate.

The relative catalytic efficiency ($k_{cat}/K_m$) of Wt GUS was found to be mostly efficient in pH range 7-8. Results suggest that substrate specificity of GUS for both PNPG and PNPGun was highest in the pH range 7-8. In case of PNPG, negatively charged C6 carboxylate interacts with positively charged active site. Although in case of PNPGun, substrate specificity of GUS seems to be slightly shifted towards the alkaline pH range of 7.5-8.5 which could possibly due to neutral C6 carboxamide in PNPGun. The results from this study confirm that GUS is mostly active and efficient in the neutral to slightly alkaline pH range.

### 3.4.2 Temperature study of Wt GUS

To investigate protein stability, Wt GUS samples were stored at different temperatures -80°C, -20°C, 4°C and 23°C (room temperature) for 4 days. The samples were run on SDS-PAGE for comparison purposes to evaluate protein degradation (**Fig 3.21**). As well, kinetic assays were performed on the samples to further probe the effects of temperature on protein activity.

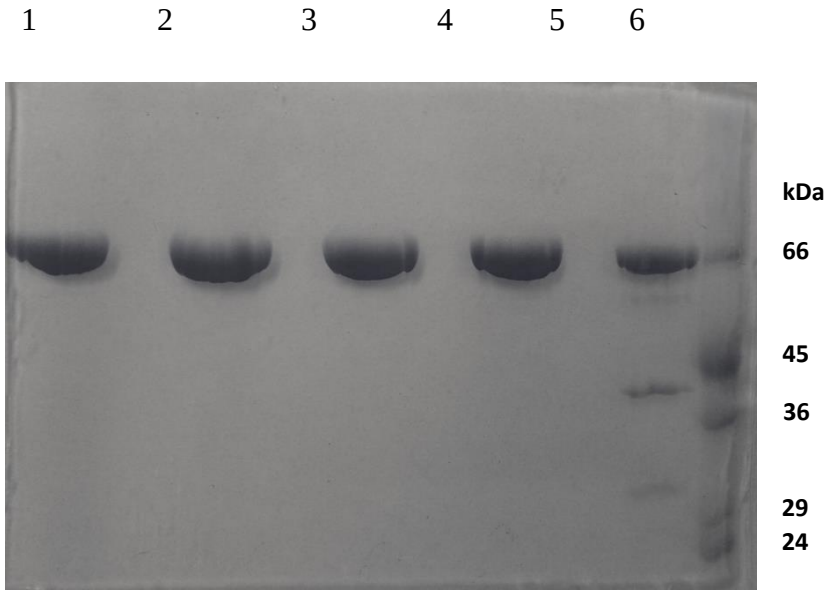


**Figure 3.21 SDS-PAGE of GUS stored under different temperatures**

Lane 1: GUS stored at -80°C. Lane 2: GUS stored at -80°C with 50% glycerol. Lane 3: GUS stored at -20°C with 50% glycerol. Lane 4: GUS stored at 4°C. Lane 5: GUS stored at room temperature. Lane 6: SDS Mol. Wt. Marker.

From the experiment, it was found that the protein samples showed similar activity while stored at different temperatures except when stored at room temperature which showed least activity (**Table 3.10**).

**Table 3.10 Kinetic parameters of Wt GUS with PNPG as substrate**

| Enzyme | Temperature | $K_m$ (mM) | $k_{cat}$ ($s^{-1}$) |
|---|---|---|---|
| **Wt GUS** | **4°C** | **0.09 ± 0.03** | **111 ± 10** |
| **Wt GUS** | **-20°C** | **0.09 ± 0.01** | **92 ± 2** |
| **Wt GUS** | **-80°C** | **0.09 ± 0.01** | **97 ± 4** |
| **Wt GUS** | **23°C (Rt*)** | **0.07 ± 0.01** | **70 ± 3** |

* Room temperature

## 3.5 Cicular Dichroism

Circular dichroism (CD) spectroscopy is a useful technique in the determination of secondary structure of protein samples. It measures differential absorption of left (L) versus right handed (R) polarized light ($\Delta A = A_L - A_R$). A CD signal will be generated when L and R component are absorbed unequally as it passes through asymmetric molecules[84]. This technique is particularly helpful in the determination of secondary structure of mutants when compared to the wild type protein[85]. It has also been used investigate structural effects which can arise from changing sample conditions such as buffer compositions, temperature and pH. The different types of regular secondary structure found in proteins give rise to characteristic CD phenomena in the far UV spectrum[86]. Peptide bonds in α-helices, β-sheets, β turns and random coils exhibit absorption below 240 nm[86]. Secondary structures such as α-helices show negative bands at 222 nm and 208 nm, and positive band at 193 nm[87, 88]. CD spectrum for β-sheets show negative bands at 218 nm and positive bands at 195 nm[89], while disordered protein structure have very low ellipticity below 210 nm and negative bands near 195 nm[90].

Site directed mutagenesis may results in disintegration of secondary structure of protein. To verify that mutations have no effect on enzyme secondary structure, CD experiments were performed.

Circular dichroism spectrums were collected in the far UV region (180-250) which corresponds to the peptide bond absorption energy. The data can be used to obtain information on the secondary structure content of protein molecules.

The reduction or elimination of catalytic activity for GUS mutants could be attributed to a deleterious change in secondary protein structure. Point mutation to the residues, which are elemental in formation of a α-helix, β-strands or β-turns, results in loss of structural integrity of protein. As neutral (glutamine) and negatively charged (glutamate) residues were introduced into the active site, the disruption of the overall charge could result in disordered secondary structure of the protein. As such, examination of the mutated GUS proteins through CD experiments was warranted.

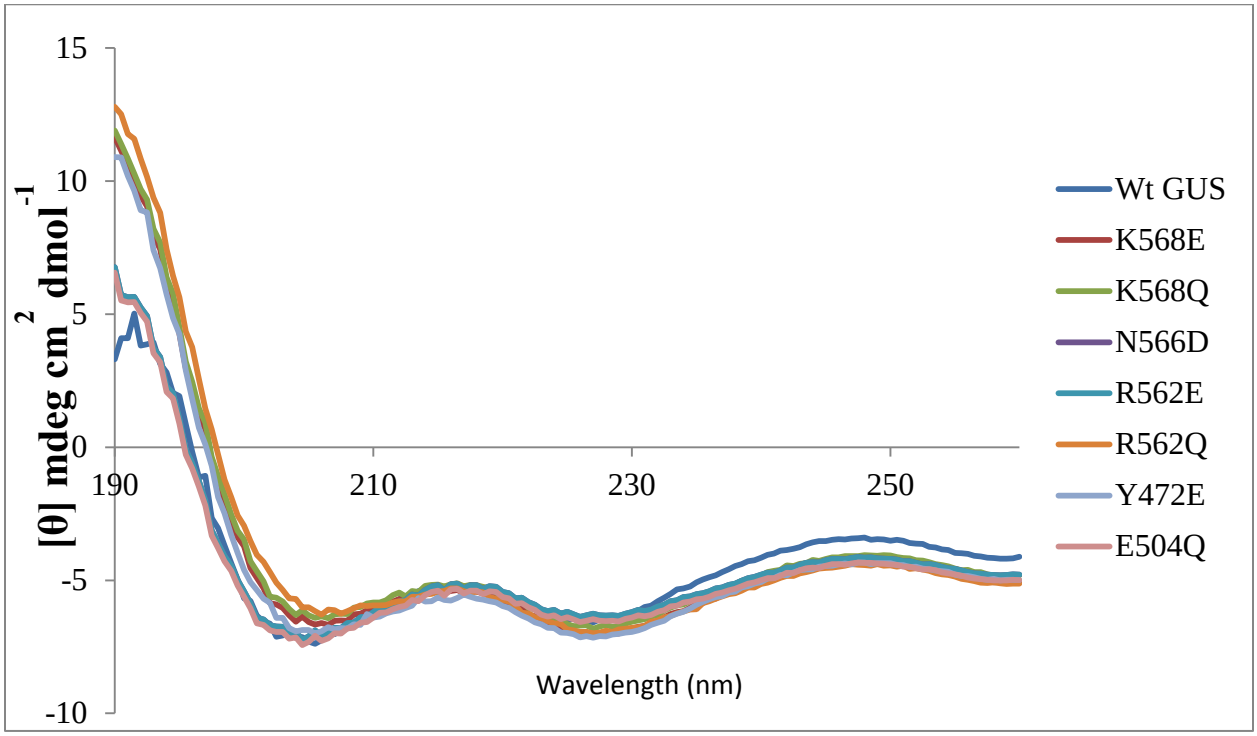


**Figure 3.22 Cicular dichroism spectrum for Wt GUS and mutants.**

[θ] corresponds to the molar ellipticity

Wt GUS and its mutants were compared with the wild type protein to confirm mutations made to the protein did not have an effect on the secondary structure (**Table 3.11** and **Fig 3.22**).

CDNN software was used to deconvolute the data which utilizes a database of known protein secondary structure information to determine the percent secondary structure content of the sample. Apart from random noise, the accepted error of the analysis of the CDNN software is between 1-5% [91].

The percent secondary structure content of the mutants was found to be comparable with Wt GUS when examined over the range of 200-260 nm. Overall, the results suggest that the loss of activity for the mutants is likely not due to significant changes in protein secondary structure, but due to the mutations itself.

**Table 3.11 Comparing secondary structure percentage content of wild type GUS and its mutants**.

| Secondary Structures | Wt GUS | E504Q | N566D | R562Q | R562E | K568Q | K568E | Y472E |
|---|---|---|---|---|---|---|---|---|
| α-helices % | 18 | 18 | 17 | 20 | 17 | 19 | 20 | 20 |
| β-antiparallel % | 23 | 24 | 24 | 21 | 24 | 22 | 21 | 21 |
| β-parallel % | 5 | 5 | 5 | 5 | 5 | 5 | 5 | 5 |
| β-Turn % | 18 | 19 | 19 | 18 | 19 | 18 | 18 | 18 |
| Random Coil % | 35 | 35 | 35 | 35 | 35 | 36 | 35 | 35 |
| Total Sum % | 99 | 101 | 100 | 99 | 100 | 100 | 99 | 99 |

## 3.6 Isothermal Titration Calorimetry

Isothermal titration calorimetry (ITC) has been widely used in study of biomolecular interactions such as protein-protein[92] and protein ligand interactions[93]. The fundamental premise

behind ITC is that heat change is always associated with these types of interactions. This observed heat change determines the affinity of the reaction[94]. Thermodynamic parameters are characterized depending on the stoichiometry of the reaction (n), enthalpy (ΔH), and binding affinity ($K_a$). Subsequently both entropy (ΔS) and free energy (ΔG) can be calculated from the measurable parameters[93]. In a typical experiment, reactant (ligand) is titrated against the protein which is present in the reaction cell. Each injection produces measurable quantity of heat (Q) which corresponds to the signal from the baseline. The heat is directly proportional to quantity of ligand binding to the protein in each injection. The binding enthalpy is calculated by integrating signal from baseline (area under curve) over the duration of each peak [95] .

An ITC instrument consists of two identical cells; a reference cell and a sample cell, composed of a highly efficient thermal conducting material (gold) surrounded by an adiabatic jacket[92]. Sensitive thermocouple circuits detect temperature differences between the two cells and between the cells and the jacket (**Fig 3.23**). Heaters located on both cells and the jacket are activated when necessary to maintain identical temperatures between all components[92].

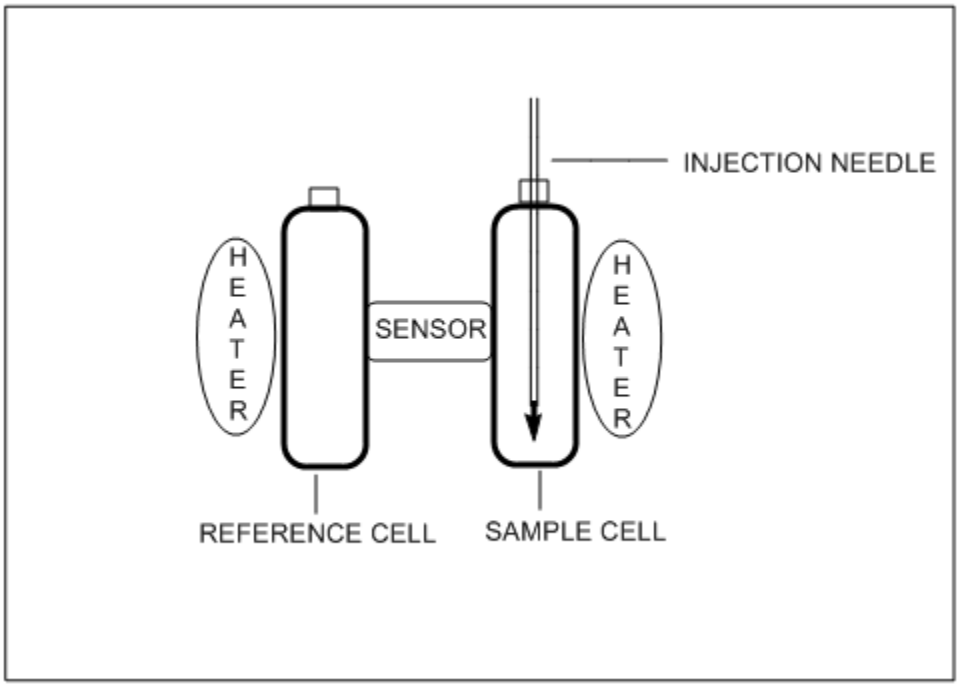


**Figure 3.23 Schematic diagram of an ITC instrument.**

The macromolecule being investigated is placed in the reaction cell and the reference cell contains only buffer. Constant power is applied to both reference and reaction cell to maintain constant temperature throughout the course of the reaction. This produces the baseline signal. Heat is taken up or released in a reaction upon ligand injections. This results in a change in temperature which is maintained by applying more power to the cells to keep the temperature constant. An exothermic reaction is based on binding affinity of ligand towards the protein. The initial ligand injections result in relatively larger peaks due to higher heat production. As ligand concentration increases in the cell, due to subsequent injections, protein saturation occurs and less heat is released. After saturation of protein, further injections generate peaks of similar magnitude (smaller), which is equivalent to the heat of dilution of ligand in buffer. A control experiment is also run by injecting ligand in the buffer without protein, to measure heat of dilution of ligand[93]. Each experiment consists of 10-20 injections of ligand depending upon the saturation rate of the macromolecule being investigated.

The ITC technique is very useful in determining ligand binding or protein interaction studies. Enthalpy driven reactions can be easily quantified, making it more versatile and sensitive towards measuring the binding isotherm of a reaction. ITC plays a vital role in ligand binding studies[96], especially in cases where no enzyme activity is showed by the amino acid mutations, ITC predicts the binding of the ligand with the enzyme.

ITC is a biophysical technique which uses heat as a signal to measure enthalpy changes directly. A high signal to noise ratio is essential for correct determination of enthalpy and binding affinity. According to Wiseman et al., the shape of a binding isotherm, for a simple one site model, changes according to the product of the association constant ($K_a$) and the (macromolecular) receptor concentration [P], which they referred to as the *c* value[97].

$$c = [P]K_a \tag{14}$$

For c values higher than 10, the binding isotherm tends to be sigmoidal in shape. Experimentally determined *c* value have an optimal range from 10-500 for good binding isotherm while c values lower than 10 are indicative of poor isotherm shape [97]. In the case of low affinity systems, the protein concentration must be high enough to achieve reasonable *c* value to generate sufficient binding isotherm for extraction of thermodynamic parameters.

Turnbull and Daranas validated that in the case of low *c* values if the stoichiometry of the reaction is known and a high signal to noise ratio and sufficient portion of binding isotherm is measured, then thermodynamic parameters like enthalpy ( $\Delta H$) and binding constant ($K_a$) can be determined accurately [98]. Advancement in ITC instrumentation in the last 10 years has allowed for weaker protein-ligand interactions which have correspondingly low c values, to be measured with increased accuracy[98].

Injections were made at an interval of 150-200 s while equilibrium was achieved within 150 s. Samples were degassed for at least an hour, as even a very small air bubble increases the noise level and the signal to noise ratio greatly perturbed.

The determination of thermodynamic parameters depends on the fitness of binding curve. A higher degree of sigmoidal curve yields more accurately thermodynamic parameters. Inaccurate protein:ligand stoichiometry can often arise due to impurity in protein samples or undetermined concentrations.

Isothermal titration calorimetry was performed on binding of glucuronic acid with Wt GUS to establish comparative enthalpic and entropic parameters. GUS substrates are specifically glucuronide derivatives. The glucuronic acid portion is vital for substrate recognition and hence catalysis. As previously discussed, mutational kinetic analysis suggested the importance of K568 for catalytic activity of PNPG. However, the data does not preclude substrate binding, merely that a productive binding mode was not achieved. ITC measurements were conducted to further probe the binding of the recognition portion of the substrate, that being glucuronic acid, with both K568Q and K568E mutants.

### 3.6.1. ITC derived thermodynamic parameters for Glucuronic acid

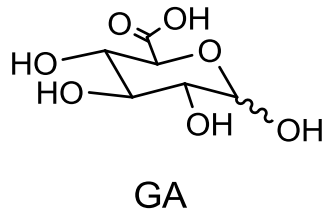


GA

**Figure 3.24 Ligand used in ITC experiments is Glucuronic acid (GA)**

Glucuronic acid (GA) (**Fig 3.24**) was used to probe binding towards GUS and to establish enthalpic and entropic contributions. Experiments were conducted at 25°C and samples were diluted for optimizing better signal to noise ratio. The $K_d$ for GA binding was determined to be 3.7 mM, which agrees well with the $K_i$ (5.6 mM) determined kinetically. The stoichiometry for protein and inhibitor was shown to be 1.0 using an independent model. The enthalpic ($\Delta H$) contribution for binding was found to be -16.78 kJ/mol and entropic ($T\Delta S$) contribution was determined to be -2.8 kJ/mol. These results indicate that GA binding was more enthalpy driven while being disfavored by entropy (**Table 3.12** and **Fig 3.25**).

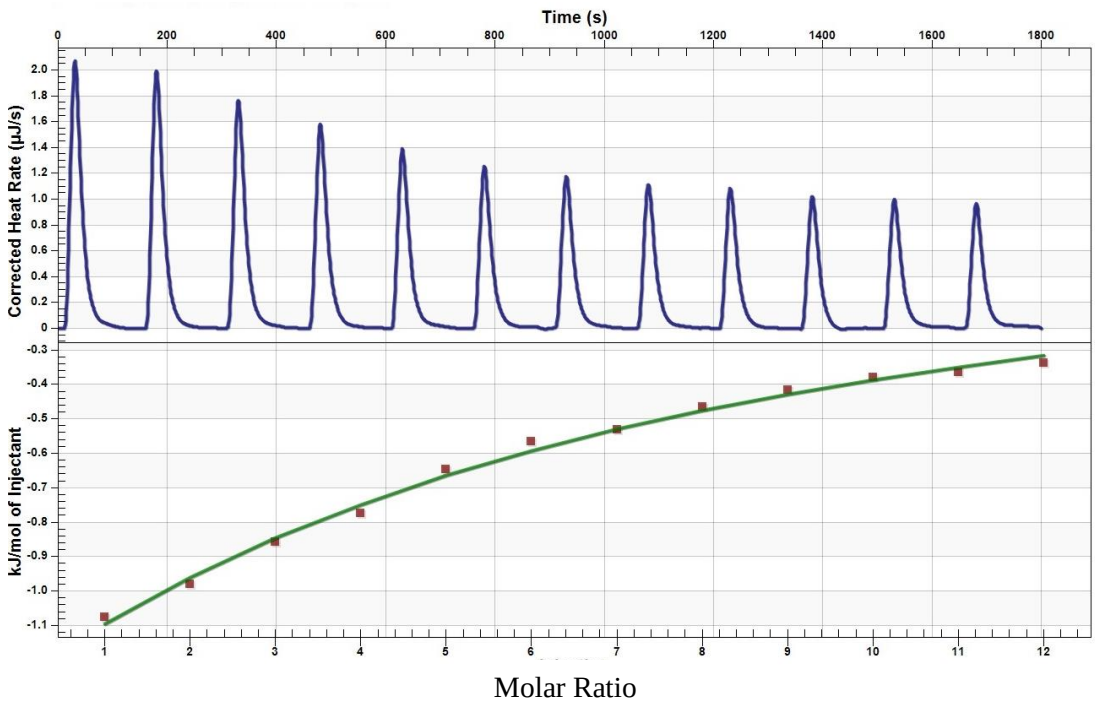


**Figure 3.25 Isothermal titration calorimetry analysis of Wt GUS with Glucuronic acid**.

Top panel shows the raw data for 12 injections (4 µL) of GA (10 mM) into buffered solution Wt GUS (0.29 mM). Bottom panel shows the fit to an independent model from Nano Analyze provided by TA instruments.

To investigate binding of GA with K568 mutants, ITC experiments were conducted under similar condition using similar concentrations of protein and ligand. Titration of GA into buffered solution of either GUS K568Q or K568E produced successive peaks of similar magnitude throughout the entire experiment (**Fig 3.26 and 3.27**). As a control experiment,

titration of GA into the same buffer without protein produced heats of dilution of similar magnitude to those observed for when K568Q or K568E were present. As such, the data indicates that GA does not bind to either of the K568Q or K568E GUS mutants within the measureable limits of the instrument. Ultimately, the results reveal the importance of the K568 residue to binding of the recognition portion (GA) of the substrate.

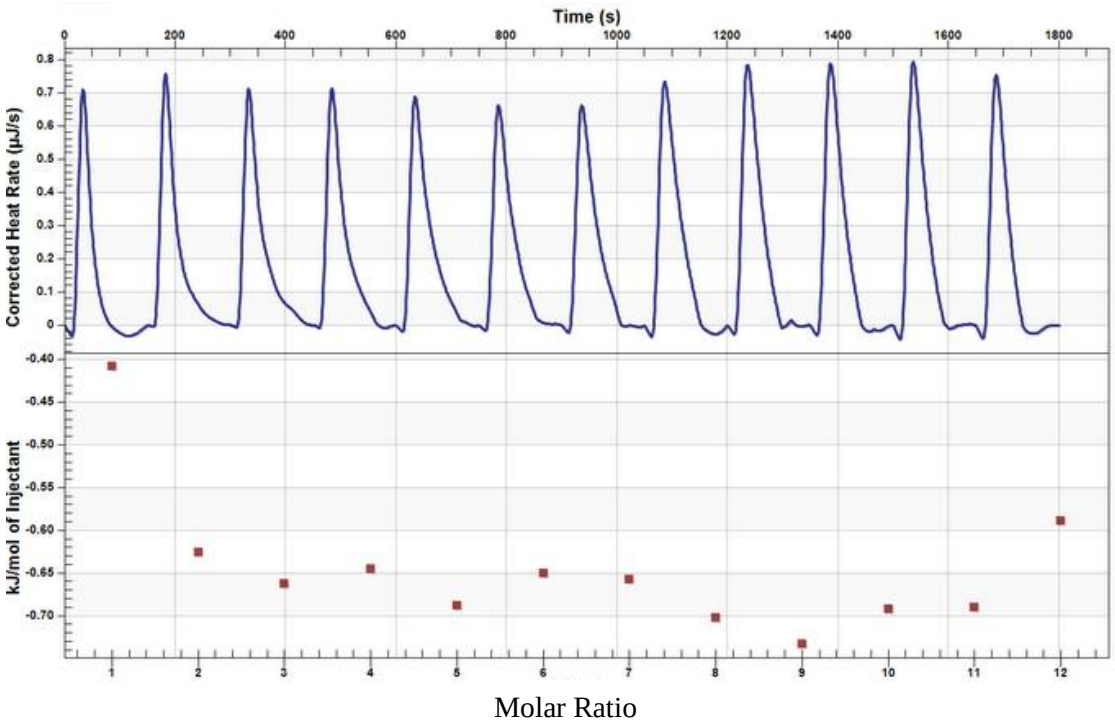


**Figure 3.26 Isothermal titration calorimetry analysis of GUS K568E with Glucuronic acid**. Top panel shows the raw data for 12 injections (4 µL) of GA (10 mM) into buffered solution GUS K568E (0.27 mM). Heat of dilution was subtracted. Bottom panel shows poor fit to an independent model from Nano Analyze provided by TA instruments

One of the parameters which can be adjusted to improve measurable signal is protein concentration. Achieving enough higher concentration to measure binding is difficult in biological systems. Efforts were made to achieve higher concentrations of protein resulted in protein precipitation and could not be resolved.

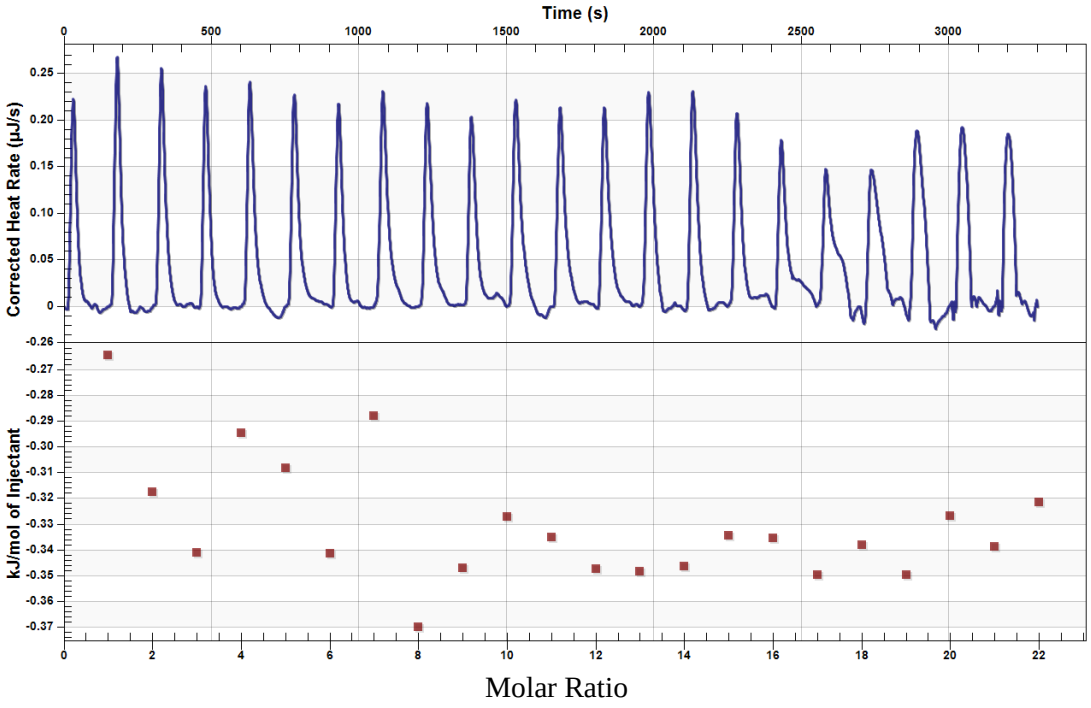


**Figure 3.27 Isothermal titration calorimetry analysis of GUS K568Q with Glucuronic acid**. Top panel shows the raw data for 22 injections (2 µL) of GA (10 mM) into buffered solution GUS K568Q (0.29 mM). Heat of dilution was subtracted .Bottom panel shows poor fit to an independent model from Nano Analyze provided by TA instruments

### 3.6.2. Thermodynamic parameters of Wt GUS with Glucaro-δ-lactam

Best inhibitors for glycosidases (glycoside hydrolase) are the ones that mimic the transition state during the substrate binding event [99]. Several substrate analogues were tested earlier to mimic the transition state in the substrate binding event including one of the known inhibitor against *E.coli* GUS is GDL (**Fig 3.28**), inhibiting strongly in the micromolar range [51, 96]. X ray structure of *E. coli* GUS bound GDL showed strong interaction with the nearby residues

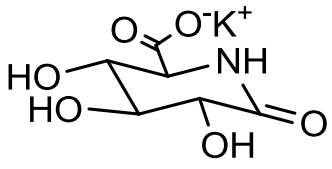


GDL

**Figure 3.28 Ligand used in ITC experiments is potassium salt of glucaro-δ-lactam (GDL)**

as discussed above. Dissecting thermodynamic parameters for GDL binding towards GUS revealed that the virtuosity of GDL binding derived not only from large enthalpic contributions (-17.5 kJ/mol) but also from large positive entropy (14.4 kJ/mol) (**Table 3.12** and **Fig 3.29**). The $K_d$ for binding was determined to be 2.7 µM, which is roughly in agreement with $K_i$ value (7.7 µM) published previously [51]. The enthalpic and entropic contribution made by GDL is in agreement with the previous published ITC studies by similar glycosidase inhibitor analogues[96, 100].

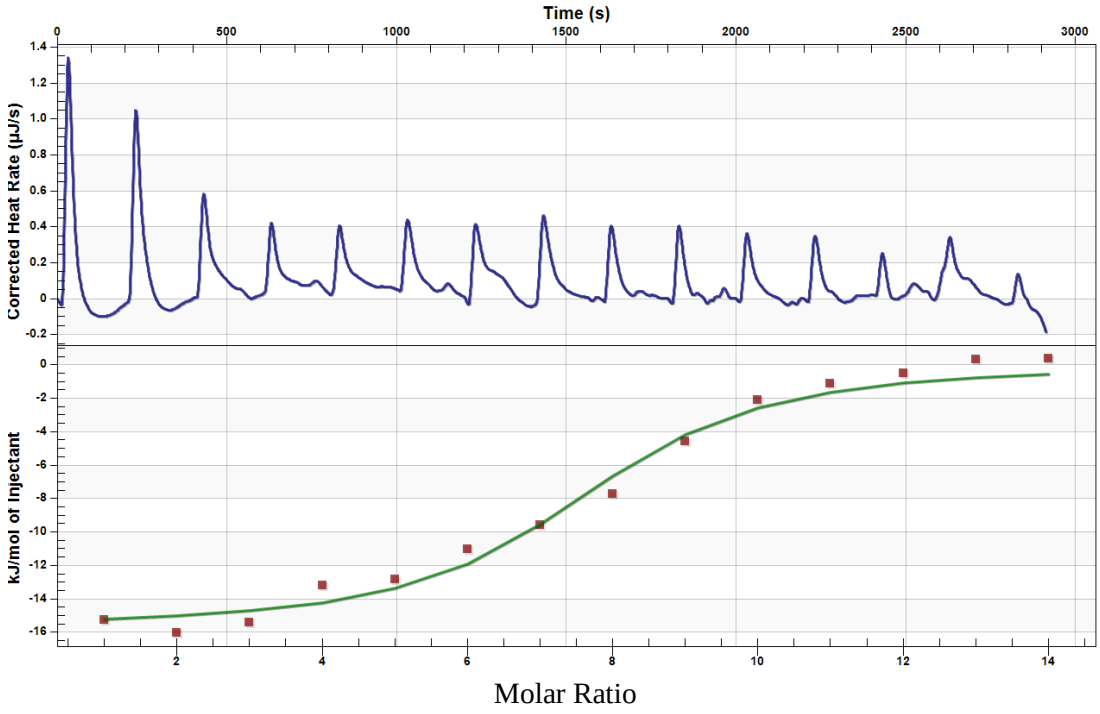


**Figure 3.29 Isothermal titration calorimetry analysis of Wt GUS with GDL**.

Top panel shows the raw data for 14 injections (2 µL) of GDL (500 µM) into buffered solution Wt GUS (50 µM). Bottom panel shows the fit to an independent model from Nano Analyze provided by TA instruments

Although it is likely that GDL binding is similar to the glucuronic acid, it is not known as there is no X ray structure of *E. coli* GUS with GA. The ITC on native GUS compared to K568 mutants will give us an idea if that residue is important to GDL binding. And if there is an effect on GDL binding due to mutation on K568, this effect could be seen with substrate binding. The binding of GDL will examine the importance of K568 residue.

### 3.6.3. Thermodynamic parameters of GUS K568E and K568Q with Glucaro-δ-lactam

The known inhibitor, GDL, was used to explore binding with mutants K568E and K568Q. Experimental result revealed that GDL binds to the mutants with a similar binding constant as it does to wild type protein. The $K_d$ value for K568E and K568Q were 2.4 µM and 7.7 µM respectively (**Table 3.12 and Fig 3.30, 3.31**).

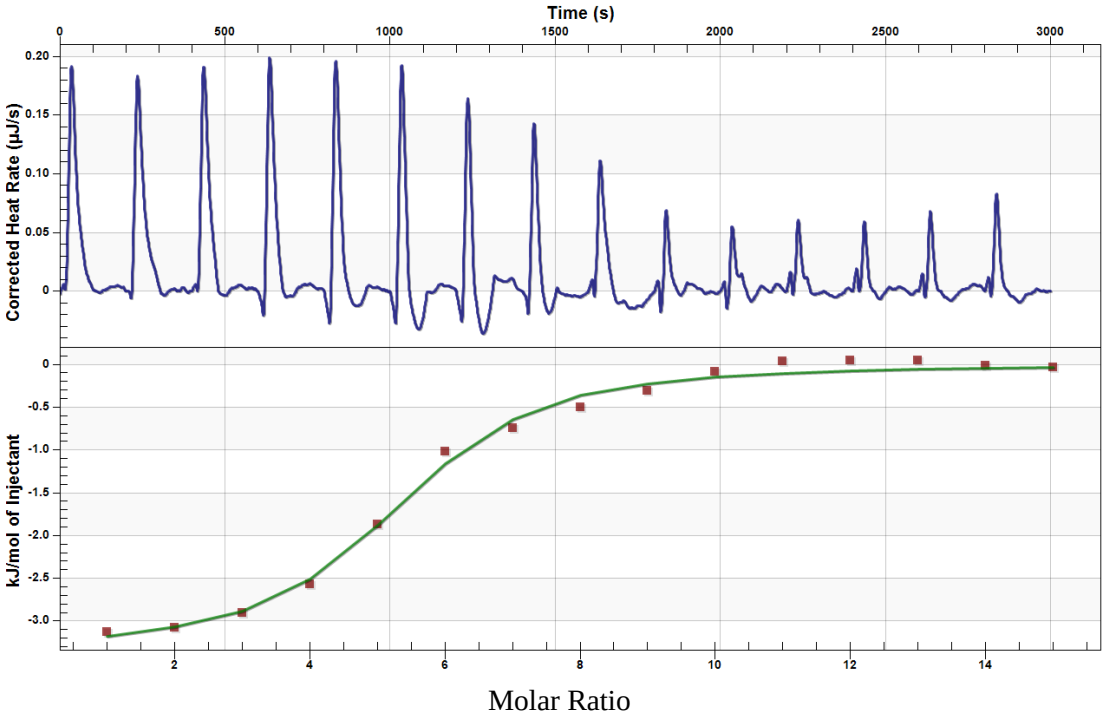


**Figure 3.30 Isothermal titration calorimetry analysis of GUS K568E with GDL**.

Top panel shows the raw data for 15 injections (3 µL) of GDL (500 µM) into buffered solution GUS K568E (50 µM). Bottom panel shows the fit to an independent model from Nano Analyze provided by TA instruments

As compared to Wt GUS, the mutant binding event was driven less by enthalpy (K568E: -6.4 kJ/mol and K568Q: -2.6 kJ/mol) and more by entropic (K568E: 25.6 kJ/mol and K568Q: 26.5 kJ/mol) contributions. The lower mutant enthalpies suggest K568 plays an important role in making strong interactions with the inhibitor. In regard to the entropy contributions, the mutants favored the overall binding of ligand to a greater extent which could signify an increased removal of solvent upon ligand binding.

High enthalpy values are often observed due to the formation of hydrogen bonds, van der Waals forces and electrostatic interactions. Deconvolution of entropic factors is more complicated due

to solvation effects of both protein and ligand and the associated rotational and translational degrees of freedom of both protein and ligand[101]. In general positive entropy is encountered when solvent molecules are released during the ligand binding event, while negative entropy results due to loss of translation, vibrational and rotational degree of freedom[101]. Entropic gain is due to the fact that water molecules no longer remain positionally confined. Upon binding to the protein, the ligand replaces the water molecules occupying the binding site and this event leads to break several hydrogen bonds with water molecules[101]. Enthalpy and entropy values compensate each other for a binding event.

In case of K568E and K568Q, replacement of water molecule results in direct interaction of ligand with protein. Steric restrictions play vital role, as a result, some parts of conformation space of ligand remain inaccessible. Ultimately the dissociation constant ($K_d$) for GDL binding within both K568 mutants and Wt protein are similar which suggests enthalpy contributions are compensated by entropy

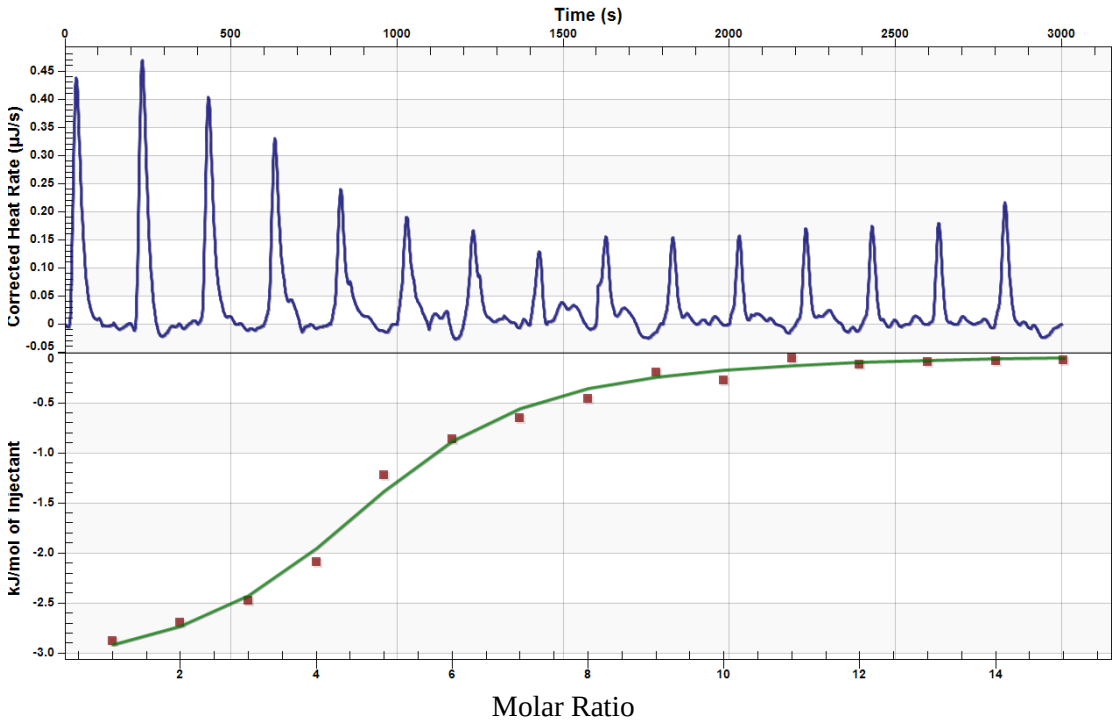


**Figure 3.31 Isothermal titration calorimetry analysis of GUS K568Q with GDL**. Top panel shows the raw data for 15 injections (3 µL) of GDL (1 mM) into buffered solution GUS K568Q (100 µM). Bottom panel shows the fit to an independent model from Nano Analyze provided by TA instruments

**Table 3.12 Isothermal titration calorimetry of Wt GUS, K568E and K568Q with glucuronic acid (GA) and Glucaro-δ-lactam (GDL)**. Each experiment was performed in triplicate at 25°C.

| Enzyme | Ligand | $K_d$ (μM) | Δ*G* (kJ/mol) | Δ*H* (kJ/mol) | TΔ*S* (kJ/mol) |
|---|---|---|---|---|---|
| **GUS** | **GA** | **(3.7 ± 1) x $10^3$** | **-13.8 ± 0.8** | **-16.78 ± 5** | **-2.8 ± 6** |
| **GUS** | **GDL** | **2.7 ± 1.5** | **-31.9 ± 1.4** | **-17.5 ± 3.3** | **14.4 ± 4.6** |
| **K568E** | **GDL** | **2.4 ± 0.2** | **-32.0 ± 0.3** | **-6.4 ± 2.7** | **25.6 ± 2.8** |
| **K568Q** | **GDL** | **7.7 ± 1.8** | **-29.1 ± 0.6** | **-2.6 ± 1.0** | **26.5 ± 1.6** |

# 4 CONCLUSION AND FUTURE WORK

## 4.1 Conclusion:

The observations of this research can be summarized as:

1. Glucuronide to glucuronamide modification reduced the overall turnover rate, which was consistently observed over *p*-nitrophenyl, phenyl and 4-methylumbelliferyl derivatives

   Wild-type GUS is still active on PNPGun. Most surprising is the low Michaelis constant, suggesting substrate binding interactions are not compromised by the substitution of the carboxyl group with a carboxamide. There is a 10-fold reduction in the substrate specificity.

   The substrate specificity of Wt GUS for phenyl-β-D-glucuronamide (PGun) is 30 fold less than Phenyl-β-D-Glucuronide (PG).

   4-Methylumbelliferyl-β-D-glucuronamide (MUGun) has 15 fold reduction in substrate specificity compared to MUG (4-methylumbelliferyl-β-D-glucuronide), verified by both UV spectroscopy and fluoro-spectroscopy

2. *p*-Nitrophenyl β-D-glucopyranoside (PNPGlu) is not a substrate for GUS and showed trace activity and very weak inhibition with $K_i$ = 5 mM.

3. *S*-Glucuronides such as *p*-nitro-thio-phenyl β-D-glucuronide (PNSPG) and thio-phenyl β-D-glucuronide (PGS) are not good substrates for GUS. PNSPG substrate specificity is 1500 fold less, compared to PNPG, while PGS is neither a substrate nor an inhibitor.

4. As expected, site-directed mutants which make the active site less positively charged, either by replacing a positively charged residue with neutral glutamines, or by replacing a neutral residue with negatively charged glutamates, results in an enzyme with much lower activity.

All mutations reduced the activity of the enzyme to less than 2%, residues Y472, R562, K568, N566D are involved in forming hydrogen bonds with the C6 carboxylate of PNPG. All mutations were deleterious as expected.

5. The mutations also lowered or abolished activity on PNPGun.

   Subsequently mutations also effected the interactions between the C6 carboxamide and respective residues in the near vicinity, resulting in no activity.

From all above results it is concluded that

1. A negatively-charged substrate is not required for GUS-catalyzed hydrolysis of the glycosidic bond.
   This has been demonstrated by using neutral glucuronamide derivatives with different leaving groups and the amide derivatives are still acting as substrates albeit with low turnover rate.
2. Alterations to the active site have a similar effect on glucuronic acid and Gun substrates

   Site directed mutagenesis results in reduced activity of enzyme against PNPG which was expected, but subsequent mutations also reduced the activity towards PNPGun.

3. Further mutational studies are required to investigate substrate selectivity exhibited by GUS

   Our initial hypothesis was that ionic interactions between negatively charged C6 carboxylate and positively charged residues Arg 562 and Lys 568 in enzyme bound structure are important for activity. Substituting a neutral carboxamide at the C6 position still acts as a substrate and in fact, binding interactions are not compromised to larger extent, suggesting further understanding of enzyme structure function relationship is required. The role of residues near the C6 carboxyl group of glucuronide such as Y469, Y468, K567, D163, and W549 still need to be explored.

A glucuronamide derivatized substrate proved to be a poor substrate for Wt GUS supported by the kinetics results. There is still a further need of finding appropriate mutations required to make glucuronamide a better substrate for the mutated version of GUS.

Purified Wt GUS was supplied to colleagues for the crystallization trials, which were not successful at the time of writing this thesis. So far, there is no crystal structure of GUS with substrate has been obtained yet. The 3-dimensional structure of GUS with substrate bound will be helpful in understanding this protein and would assist in modifying substrate specificity.

## 4.2 Future Work

Residues near the active site are frequently involved in substrate specificity and may improve kinetics. There is a further need of finding appropriate mutations required to make PNPGun a good substrate. PNPGun still binds to the Wt GUS and shows activity which suggests further improvement in substrate modification are required so that native enzyme will not be able recognize the substrate. Further substrate modification could be implementing methyl or ethyl ester at C6 position.

Limited mutations were not successful to unravel the residues roles in substrate specificity and in regaining activity against PNPGun as a better substrate. Point mutations to residues Y472, Y468, D163, and N566 to positively charged residues such as arginine or lysine will make the active site more positively charged and could be beneficial.

So far there is no GUS structure with substrate is available, X ray crystal structure of GUS with substrate would open the gates in uncovering the residues roles responsible for substrate interactions. This would also help in further understanding of structure function relationship of GUS.

Kinetic study needs to be performed on human GUS using amide derivatized substrate to verify if the effects are the same as in the case of *E. coli* GUS. Once the base research goal is established, the principles will be translated to human GUS to reduce the chance of immunogenic response for ADEPT.

# 5 REFERENCES


1. Shukla, G. S.; Krag, D. N., **2006,** Selective delivery of therapeutic agents for the diagnosis and treatment of cancer. *Expert Opinion on Biological Therapy***,** *6* (1), 39-54.
2. Mehra, N. K., *et al.*, **2013,** Receptor-based targeting of therapeutics. *Therapeutic Delivery***,** *4* (3), 369-394.
3. Bagshawe, K. D., **1989,** The first Bagshawe lecture. Towards generating cytotoxic agents at cancer sites. *British journal of cancer***,** *60* (3), 275-281.
4. Xu, G.; McLeod, H. L., **2001,** Strategies for enzyme/prodrug cancer therapy. *Clinical Cancer Research***,** *7* (11), 3314-3324.
5. Niculescu-Duvaz, I.; Springer, C. J., **1997,** Gene-directed enzyme prodrug therapy. *Expert Opinion on Investigational Drugs***,** *6* (6), 685-704.
6. Khatri, A., *et al.*, **2006,** Combination of cytosine deaminase with uracil phosphoribosyl transferase leads to local and distant bystander effects against RM1 prostate cancer in mice. *The Journal of Gene Medicine***,** *8* (9), 1086-1096.
7. Marais, R., *et al.*, **1996,** Gene-directed enzyme prodrug therapy with a mustard prodrug/carboxypeptidase G2 combination. *Cancer Research***,** *56* (20), 4735-4742.
8. McCarthy, H. O., *et al.*, **2003,** Bioreductive gdept using cytochrome P450 3A4 in combination with AQ4N. *Cancer Gene Ther***,** *10* (1), 40-48.
9. Schellmann, N., *et al.*, **2010,** Targeted enzyme prodrug therapies. *Mini Rev Med Chem***,** *10* (10), 887-904.
10. Kwiatkowska, A., *et al.*, **2013,** Strategies in gene therapy for glioblastoma. *Cancers***,** *5* (4), 1271-1305.
11. Okabe, S., *et al.*, **2003,** Adenovirus-mediated prodrug-enzyme therapy for CEA-producing colorectal cancer cells. *Journal of Cancer Research and Clinical Oncology***,** *129* (6), 367-373.
12. Martiniello-Wilks, R., *et al.*, **2002,** Transcription-targeted gene therapy for androgen-independent prostate cancer. *Cancer Gene Ther***,** *9* (5), 443-452.
13. Hamstra, D. A., *et al.*, **1999,** Enzyme/prodrug therapy for head and neck cancer using a catalytically superior cytosine deaminase. *Hum Gene Ther***,** *10* (12), 1993-2003.

14. Bagshawe, K. D., *et al.*, **1988,** A cytotoxic agent can be generated selectively at cancer sites. *Br J Cancer***,** *58* (6), 700-703.

15. Bagshawe, K. D., *et al.*, **1994,** Antibody Directed Enzyme Prodrug Therapy (adept): A review of some theoretical, experimental and clinical aspects. *Annals of Oncology***,** *5* (10), 879-891.

16. Bodey, B., **2001,** Genetically engineered antibodies for direct antineoplastic treatment and systematic delivery of various therapeutic agents to cancer cells. *Expert Opinion on Biological Therapy***,** *1* (4), 603-617.

17. MacDonald, G. C.; Glover, N., **2005,** Effective tumor targeting: Strategies for the delivery of armed antibodies. *Curr Opin Drug Discov Devel***,** *8* (2), 177-183.

18. Bernard-Marty, C., *et al.*, **2006,** Monoclonal antibody-based targeted therapy in breast cancer. *Drugs***,** *66* (12), 1577-1591.

19. Mayer, I. A., **2009,** Treatment of HER2-positive metastatic breast cancer following initial progression. *Clinical Breast Cancer***,** *9, Supplement 2* (0), S50-S57.

20. Roskoski Jr, R., **2004,** The ErbB/HER receptor protein-tyrosine kinases and cancer. *Biochemical and Biophysical Research Communications***,** *319* (1), 1-11.

21. Hay, M. P., *et al.*, **1995,** A novel enediyne prodrug for antibody-directed enzyme prodrug therapy (ADEPT) using e. Coli b nitroreductase. *Bioorganic & Medicinal Chemistry Letters***,** *5* (23), 2829-2834.

22. Deckert, P. M., *et al.*, **2004,** Specific tumour localisation of a huA33 antibody--carboxypeptidase a conjugate and activation of methotrexate-phenylalanine. *International journal of oncology***,** *24* (5), 1289-1295.

23. Alexander, R. P., *et al.*, **1991,** Cephalosporin nitrogen mustard carbamate prodrugs for "ADEPT". *Tetrahedron Letters***,** *32* (27), 3269-3272.

24. Francis, R. J., *et al.*, **2002,** A phase i trial of antibody directed enzyme prodrug therapy (adept) in patients with advanced colorectal carcinoma or other CEA producing tumours. *British journal of cancer***,** *87* (6), 600-607.

25. Houba, P. H. J., *et al.*, **2001,** A novel doxorubicin-glucuronide prodrug DOX-GA3 for tumour-selective chemotherapy: Distribution and efficacy in experimental human ovarian cancer. *Br J Cancer***,** *84* (4), 550-557.

26. Kim, K., *et al.*, **2003,** Membrane-bound alkaline phosphatase gene induces antitumor effect by G2/M arrest in etoposide phosphate-treated cancer cells. *Molecular and Cellular Biochemistry*, *252* (1-2), 213-221.

27. Gesson, J. P., *et al.*, **1994,** Prodrugs of anthracyclines for chemotherapy via enzyme-monoclonal antibody conjugates. *Anticancer Drug Des*, *9* (5), 409-423.

28. Vrudhula, V. M., *et al.*, **1993,** Prodrugs of doxorubicin and melphalan and their activation by a monoclonal antibody-penicillin-G amidase conjugate. *Journal of Medicinal Chemistry*, *36* (7), 919-923.

29. Niculescu-Duvaz, I.; Springer, C. J., **1997,** Antibody-directed enzyme prodrug therapy (ADEPT): A review. *Advanced Drug Delivery Reviews*, *26* (2–3), 151-172.

30. Denny, W. A.; Wilson, W. R., **1998,** The design of selectively-activated anti-cancer prodrugs for use in antibody-directed and gene-directed enzyme-prodrug therapies. *Journal of Pharmacy and Pharmacology*, *50* (4), 387-394.

31. Senter, P. D., *et al.*, **1993,** Generation of cytotoxic agents by targeted enzymes. *Bioconjugate Chemistry*, *4* (1), 3-9.

32. Miller, R. D., *et al.*, **1990,** Cloning and characterization of the human β-glucuronidase gene. *Genomics*, *7* (2), 280-283.

33. Jefferson, R. A., *et al.*, **1986,** Beta-glucuronidase from Escherichia coli as a gene-fusion marker. *Proc Natl Acad Sci U S A*, *83* (22), 8447-8451.

34. Bosslet, K., *et al.*, **1992,** Molecular and functional characterisation of a fusion protein suited for tumour specific prodrug activation. *Br J Cancer*, *65* (2), 234-238.

35. Erickson-Miller, C. L., *et al.*, **1997,** Differential toxicity of camptothecin, topotecan and 9-aminocamptothecin to human, canine, and murine myeloid progenitors (CFU-GM) in vitro. *Cancer Chemother Pharmacol*, *39* (5), 467-472.

36. Haisma, H. J., *et al.*, **1994,** Comparison of two anthracycline-based prodrugs for activation by a monoclonal antibody-beta-glucuronidase conjugate in the specific treatment of cancer. *Cell Biophys*, *24-25*, 185-192.

37. Unak, T., **2000,** Potential use of radiolabeled glucuronide prodrugs with auger and/or alpha emitters in combined chemo- and radio-therapy of cancer. *Curr Pharm Des*, *6* (11), 1127-1142.

38. Chen, X., *et al.*, **2003,** Glucuronides in anti-cancer therapy. *Current Medicinal Chemistry -Anti-Cancer Agents***,** *3* (2), 139-150.

39. Chen, K.-C., *et al.*, **2008,** Directed evolution of a lysosomal enzyme with enhanced activity at neutral pH by mammalian cell-surface display. *Chemistry & biology***,** *15* (12), 1277-1286.

40. Eccles, S. A., *et al.*, **1994,** Regression of established breast carcinoma xenografts with antibody-directed enzyme prodrug therapy against c-erbb2 p185. *Cancer Research***,** *54* (19), 5171-5177.

41. Bagshawe, K. D., *et al.*, **2004,** Antibody-directed enzyme prodrug therapy (adept) for cancer. *Expert Opin Biol Ther***,** *4* (11), 1777-1789.

42. Bagshawe, K. D., **2009,** Targeting: The ADEPT story so far. *Current Drug Targets***,** *10* (2), 152-157.

43. Meyer, K., *et al.*, **1951,** The production of monosaccharides from hyaluronic acid by β-glucuronidase. *Journal of Biological Chemistry***,** *192* (1), 275-281.

44. Matsumura, I.; Ellington, A. D., **2001,** In vitro evolution of beta-glucuronidase into a beta-galactosidase proceeds through non-specific intermediates. *Journal of Molecular Biology***,** *305* (2), 331-339.

45. Wang, C.-C.; Touster, O., **1972,** Studies of catalysis by β-glucuronidase: The effect of structure on the rate of hydrolysis of substituted phenyl-β-D-glucopyranosiduronic acids. *Journal of Biological Chemistry***,** *247* (9), 2650-2656.

46. Okkels, F. T., *et al.*, **1997,** Synthesis of cytokinin glucuronides for the selection of transgenic plant cells. *Phytochemistry***,** *46* (5), 801-804.

47. Islam, M. R., *et al.*, **1999,** Active site residues of human β-glucuronidase: Evidence for glu540 as the nucleophile and glu451 as the acid-base residue. *Journal of Biological Chemistry***,** *274* (33), 23451-23455.

48. Salleh, H. M., *et al.*, **2006,** Cloning and characterization of thermotoga maritima β-glucuronidase. *Carbohydrate Research***,** *341* (1), 49-59.

49. Michikawa, M., *et al.*, **2012,** Structural and biochemical characterization of glycoside hydrolase family 79 β-glucuronidase from acidobacterium capsulatum. *Journal of Biological Chemistry***,** *287* (17), 14069-14077.

50. Jain, S., *et al.*, **1996,** Structure of human beta-glucuronidase reveals candidate lysosomal targeting and active-site motifs. *Nat Struct Biol***,** *3* (4), 375-381.

51. Wallace, B. D., *et al.*, **2010,** Alleviating cancer drug toxicity by inhibiting a bacterial enzyme. *Science***,** *330* (6005), 831-835.

52. Xiong, A.-S., *et al.*, **2007,** Concurrent mutations in six amino acids in β-glucuronidase improve its thermostability. *Protein Engineering Design and Selection***,** *20* (7), 319-325.

53. Jefferson, R. A., *et al.*, **1987,** Gus fusions: Beta-glucuronidase as a sensitive and versatile gene fusion marker in higher plants. *The EMBO journal***,** *6* (13), 3901-3907.

54. Paigen, K., **1989,** Mammalian beta-glucuronidase: Genetics, molecular biology, and cell biology. *Prog Nucleic Acid Res Mol Biol***,** *37*, 155-205.

55. Sperker, B., *et al.*, **1997,** Interindividual variability in expression and activity of human β-glucuronidase in liver and kidney: Consequences for drug metabolism. *Journal of Pharmacology and Experimental Therapeutics***,** *281* (2), 914-920.

56. Brot, F. E., *et al.*, **1978,** Purification and properties of beta-glucuronidase from human placenta. *Biochemistry***,** *17* (3), 385-391.

57. Sly, W. S., *et al.*, **1973,** Beta glucuronidase deficiency: Report of clinical, radiologic, and biochemical features of a new mucopolysaccharidosis. *J Pediatr***,** *82* (2), 249-257.

58. Erickson, A. H.; Blobel, G., **1983,** Carboxyl-terminal proteolytic processing during biosynthesis of the lysosomal enzymes beta-glucuronidase and cathepsin d. *Biochemistry***,** *22* (22), 5201-5205.

59. Shipley, J. M., *et al.*, **1993,** The role of glycosylation and phosphorylation in the expression of active human beta-glucuronidase. *Journal of Biological Chemistry***,** *268* (16), 12193-12198.

60. Gehrmann, M. C., *et al.*, **1994,** Biochemical properties of recombinant human beta-glucuronidase synthesized in baby hamster kidney cells. *Biochem J***,** *301 ( Pt 3)*, 821-828.

61. Roberts, A. B., *et al.*, **2013,** Molecular insights into microbial β-glucuronidase inhibition to abrogate CPT-11 toxicity. *Molecular Pharmacology***,** *84* (2), 208-217.

62. Thompson, J. D., *et al.*, **1994,** Clustal-w - improving the sensitivity of progressive multiple sequence alignment through sequence weighting, position-specific gap penalties and weight matrix choice. *Nucleic Acids Research***,** *22* (22), 4673-4680.

63. Henikoff, S.; Henikoff, J. G., **1992,** Amino-acid substitution matrices from protein blocks. *Proceedings of the National Academy of Sciences of the United States of America***,** *89* (22), 10915-10919.

64. Henikoff, J. G.; Henikoff, S., [6] blocks database and its applications. In *Methods in enzymology*, Russell, F. D., Ed. Academic Press: 1996; Vol. Volume 266, pp 88-105.

65. Gouet, P., *et al.*, **1999,** Espript: Analysis of multiple sequence alignments in postscript. *Bioinformatics***,** *15* (4), 305-308.

66. Jacobson, R. H., *et al.*, **1994,** Three-dimensional structure of beta-galactosidase from e. Coli. *Nature***,** *369* (6483), 761-766.

67. Jones, G., *et al.*, **1997,** Development and validation of a genetic algorithm for flexible docking. *Journal of Molecular Biology***,** *267* (3), 727-748.

68. Xiong, A. S., *et al.*, **2007,** Directed evolution of beta-galactosidase from escherichia coli into beta-glucuronidase. *J Biochem Mol Biol***,** *40* (3), 419-425.

69. Bohm, G., *et al.*, **1992,** Quantitative analysis of protein far uv circular dichroism spectra by neural networks. *Protein Eng***,** *5* (3), 191-195.

70. Wu, X., *et al.*, **1998,** Sensitive method for the quantification of β-glucuronidase activity in human urine using capillary electrophoresis with fluorescence detection. *Journal of Chromatography B: Biomedical Sciences and Applications***,** *708* (1–2), 61-66.

71. Richard, J. P., *et al.*, **1996,** Structure−reactivity relationships for β-galactosidase (escherichia coli, lac z). 3. Evidence that glu-461 participates in brønsted acid−base catalysis of β-d-galactopyranosyl group transfer. *Biochemistry***,** *35* (38), 12377-12386.

72. Aich, S., *et al.*, **2001,** Continuous spectrophotometric assay for beta-glucuronidase. *BioTechniques***,** *30* (4), 846-850.

73. Geddie, M. L.; Matsumura, I., **2004,** Rapid evolution of β-glucuronidase specificity by saturation mutagenesis of an active site loop. *Journal of Biological Chemistry***,** *279* (25), 26462-26468.

74. Smith, W., *et al.*, **2011,** Applying neutral drift to the directed molecular evolution of a beta-glucuronidase into a beta-galactosidase: Two different evolutionary pathways lead to the same variant. *BMC Research Notes***,** *4* (1), 138.

75. Rowe, L. A., *et al.*, **2003,** A comparison of directed evolution approaches using the β-glucuronidase model system. *Journal of Molecular Biology***,** *332* (4), 851-860.

76. Flores, H.; Ellington, A. D., **2002,** Increasing the thermal stability of an oligomeric protein, beta-glucuronidase. *Journal of Molecular Biology***,** *315* (3), 325-337.

77. Narine, A. A., *et al.*, **2006,** Mechanistic requirements for the efficient enzyme-catalyzed hydrolysis of thiosialosides†. *Biochemistry***,** *45* (30), 9319-9326.

78. Hetu, C.; Gianetto, R., **1970,** Synthetic 1-thio-D-glucosiduronic acids as substrates for rat-liver -glucuronidase. *Can J Biochem***,** *48* (7), 799-804.

79. Shen, H.; Byers, L. D., **2007,** Thioglycoside hydrolysis catalyzed by beta-glucosidase. *Biochemical and Biophysical Research Communications***,** *362* (3), 717-720.

80. Vuppugalla, R., *et al.*, **2007,** Effect of commonly used organic solvents on the kinetics of cytochrome P450 2B6- and 2C8-dependent activity in human liver microsomes. *Drug Metabolism and Disposition***,** *35* (11), 1990-1995.

81. Jahn, M., *et al.*, **2003,** Thioglycoligases: Mutant glycosidases for thioglycoside synthesis. *Angewandte Chemie International Edition***,** *42* (3), 352-354.

82. Glaser, J. H.; Conrad, H. E., **1980,** Multiple kinetic forms of beta-glucuronidase. *Journal of Biological Chemistry***,** *255* (5), 1879-1894.

83. Sasaki, K., *et al.*, **2000,** Molecular characterization of a novel β-glucuronidase fromscutellaria baicalensis georgi. *Journal of Biological Chemistry***,** *275* (35), 27466-27472.

84. Lin, K., *et al.*, **2013,** Overestimated accuracy of circular dichroism in determining protein secondary structure. *European Biophysics Journal***,** *42* (6), 455-461.

85. Woody, A. Y. M.; Woody, R. W., **2003,** Individual tyrosine side-chain contributions to circular dichroism of ribonuclease. *Biopolymers***,** *72* (6), 500-513.

86. Kelly, S. M., *et al.*, **2005,** How to study proteins by circular dichroism. *Biochimica et Biophysica Acta (BBA) - Proteins and Proteomics***,** *1751* (2), 119-139.

87. Holzwarth, G.; Doty, P., **1965,** The ultraviolet circular dichroism of polypeptides. *J Am Chem Soc***,** *87*, 218-228.

88. Whitmore, L.; Wallace, B. A., **2008,** Protein secondary structure analyses from circular dichroism spectroscopy: Methods and reference databases. *Biopolymers***,** *89* (5), 392-400.

89. Greenfield, N. J.; Fasman, G. D., **1969,** Computed circular dichroism spectra for the evaluation of protein conformation. *Biochemistry***,** *8* (10), 4108-4116.

90. Venyaminov, S. Y., *et al.*, **1993,** Circular dichroic analysis of denatured proteins: Inclusion of denatured proteins in the reference set. *Analytical Biochemistry***,** *214* (1), 17-24.

91. Böhm, G., *et al.*, **1992,** Quantitative analysis of protein far uv circular dichroism spectra by neural networks. *Protein Eng, 5* (3), 191-195.

92. Pierce, M. M., *et al.*, **1999,** Isothermal titration calorimetry of protein–protein interactions. *Methods, 19* (2), 213-221.

93. Damian, L., Isothermal titration calorimetry for studying protein–ligand interactions. In *Protein-ligand interactions*, Williams, M. A.; Daviter, T., Eds. Humana Press: 2013; Vol. 1008, pp 103-118.

94. Liang, Y., **2006,** Applications of isothermal titration calorimetry in protein folding and molecular recognition. *Journal of the Iranian Chemical Society, 3* (3), 209-219.

95. Tellinghuisen, J., **2012,** Designing isothermal titration calorimetry experiments for the study of 1:1 binding: Problems with the "standard protocol". *Analytical Biochemistry, 424* (2), 211-220.

96. Gloster, T. M., *et al.*, **2007,** Glycosidase inhibition: An assessment of the binding of 18 putative transition-state mimics. *Journal of the American Chemical Society, 129* (8), 2345-2354.

97. Wiseman, T., *et al.*, **1989,** Rapid measurement of binding constants and heats of binding using a new titration calorimeter. *Analytical Biochemistry, 179* (1), 131-137.

98. Turnbull, W. B.; Daranas, A. H., **2003,** On the value of c: Can low affinity systems be studied by isothermal titration calorimetry? *Journal of the American Chemical Society, 125* (48), 14859-14866.

99. Gloster, T. M.; Davies, G. J., **2010,** Glycosidase inhibition: Assessing mimicry of the transition state. *Organic & Biomolecular Chemistry, 8* (2), 305-320.

100. Gloster, T. M., *et al.*, **2004,** Structural, thermodynamic, and kinetic analyses of tetrahydrooxazine-derived inhibitors bound to β-glucosidases. *Journal of Biological Chemistry, 279* (47), 49236-49242.

101. Klebe, G.; Bohm, H. J., **1997,** Energetic and entropic factors determining binding affinity in protein-ligand complexes. *J Recept Signal Transduct Res, 17* (1-3), 459-473.